Weak lensing for precision cosmology

Rachel Mandelbaum[1]

[1]McWilliams Center for Cosmology, Department of Physics, Carnegie Mellon University, Pittsburgh, PA 15213, USA; email: rmandelb@andrew.cmu.edu

Abstract

Weak gravitational lensing, the deflection of light by mass, is one of the best tools to constrain the growth of cosmic structure with time and reveal the nature of dark energy. I discuss the sources of systematic uncertainty in weak lensing measurements and their theoretical interpretation, including our current understanding and other options for future improvement. These include long-standing concerns such as the estimation of coherent shears from galaxy images or redshift distributions of galaxies selected based on photometric redshifts, along with systematic uncertainties that have received less attention to date because they are subdominant contributors to the error budget in current surveys. I also discuss methods for automated systematics detection using survey data of the 2020s. The goal of this review is to describe the current state of the field and what must be done so that if weak lensing measurements lead toward surprising conclusions about key questions such as the nature of dark energy, those conclusions will be credible.

Contents

1. INTRODUCTION

Gravitational lensing is the deflection of light rays from distant objects by the matter – including dark matter – along their path to us. In the limit that the deflections cause small modifications of the object properties (position, size, brightness, and shape) but not visually striking phenomena such as multiple images or arcs, lensing is referred to as "weak lensing" (for recent reviews, see Kilbinger 2015; Dodelson 2017). Since light from distant sources that are near each other on the sky must pass by nearby structures in the cosmic web (see Figure 1), their shapes are correlated by lensing. This correlation drops with separation on the sky; its amplitude and scale-dependence can be used to infer the underlying statistical distribution of matter and hence the growth of cosmic structure with time. This in turn allows us to infer the properties of dark energy (for early work along these lines, see Hu 2002; Huterer 2002), because the accelerated expansion of the Universe that it causes suppresses the clustering of matter driven by gravity.

The recognition that weak lensing provides the power to constrain the cause of the accelerated expansion rate of the Universe has driven the development of ever-larger weak lensing surveys; see e.g., the Dark Energy Task Force report (Albrecht et al. 2006) and 2010 decadal survey (Decadal Survey Committee 2010). However, weak lensing can also be used to study the galaxy-dark matter halo connection (e.g., Coupon et al. 2015; Hudson et al. 2015; van Uitert et al. 2015; Mandelbaum et al. 2016) and constrain neutrino masses (e.g., Abazajian & Dodelson 2003; Abazajian et al. 2011; DES Collaboration et al. 2017).

The correlation function of galaxy shapes (shear-shear correlations) is often referred to as 'cosmic shear'. Making these measurements requires (1) the analysis of images to
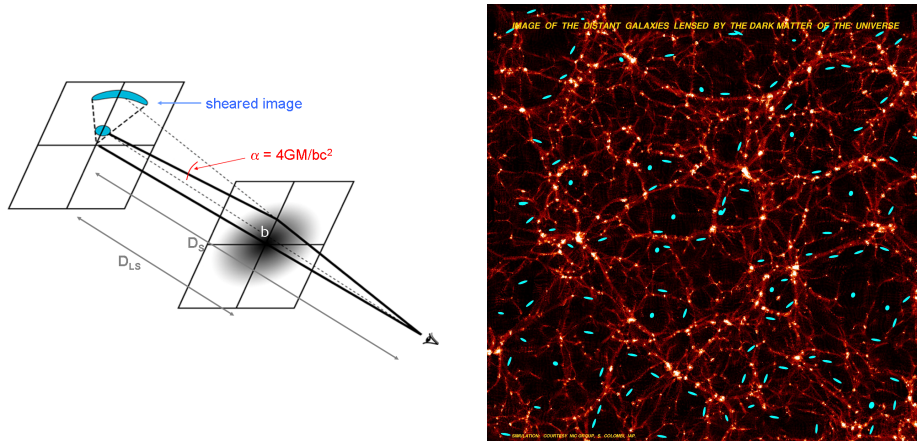
Figure 1: The left panel (from LSST Science Collaboration et al. 2009, used with permission from image creator, Tony Tyson) illustrates the basic lensing shear distortion caused by weak gravitational lensing, for a single lens and source. The right panel (image credit: Canada-France Hawaii Telescope) shows the coherent patterns induced in source shapes (blue ellipses) due to large-scale structure; the color scale indicates the density in the simulation.

infer the weak lensing distortions ('shear'), where deviations from purely random galaxy orientations are assumed to arise due to lensing; (2) estimates of distances to the galaxies involved, in order to interpret the shape distortions in terms of cosmological parameters; and (3) a host of supporting data e.g. to confirm the calibration of the redshift estimates and inferred shear. Interpreting them requires the ability to make predictions about the growth of cosmic structure at late times, well into the nonlinear regime.

Weak lensing can be described as a linear transformation between unlensed (x_u, y_u) and lensed coordinates (x_l, y_l), where the origins of the coordinate systems are at the unlensed and lensed positions of the galaxy:

$$\begin{pmatrix} x_u \\ y_u \end{pmatrix} = \begin{pmatrix} 1 - \gamma_1 - \kappa & -\gamma_2 \\ -\gamma_2 & 1 + \gamma_1 - \kappa \end{pmatrix} \begin{pmatrix} x_l \\ y_l \end{pmatrix}. \tag{1}$$

There are two components of the complex-valued lensing shear $\gamma = \gamma_1 + i\gamma_2$, which describes the stretching of galaxy images due to lensing, and the convergence κ, which describes a change in size and brightness of lensed objects. The shear has elliptical symmetry, and hence transforms like a spin-2 quantity. Since we do not know the unlensed distribution of galaxy sizes very precisely, it is common to write this as

$$\begin{pmatrix} x_u \\ y_u \end{pmatrix} = (1 - \kappa) \begin{pmatrix} 1 - g_1 & -g_2 \\ -g_2 & 1 + g_1 \end{pmatrix} \begin{pmatrix} x_l \\ y_l \end{pmatrix}, \tag{2}$$

in terms of the reduced shear, $g_i = \gamma_i/(1 - \kappa)$.

Since the lensing shear causes a change the observed galaxy ellipticities, inference of the shear typically depends on measurements of the second moments of galaxies:

$$Q_{ij} = \frac{\int d^2x\, I(\mathbf{x})W(\mathbf{x})x_i x_j}{\int d^2x\, I(\mathbf{x})W(\mathbf{x})}, \tag{3}$$

where x_1 and x_2 correspond to the x and y directions, $I(\mathbf{x})$ denotes the galaxy image light profile, and $W(\mathbf{x})$ is a weighting function. One common definition of ellipticity relates to the moments as

$$e = e_1 + \mathrm{i}e_2 = \frac{Q_{11} - Q_{22} + 2\mathrm{i}Q_{12}}{Q_{11} + Q_{22}}. \tag{4}$$

Another definition of ellipticity replaces the denominator in Eq. 4 with $Q_{11} + Q_{22} + 2[\det(Q)]^{1/2}$. Both ellipticity definitions have a well-defined response to a lensing shear, and hence can be averaged across ensembles of galaxies. A variety of methods exist for estimating these ellipticities while removing the effect of the point-spread function (PSF) from the atmosphere and telescope.

The convergence can be thought of as the projected matter overdensity, defined for a given point on the sky θ as

$$\kappa(\theta) = \frac{3H_0^2 \Omega_m}{2c^2} \int_0^\chi \frac{\mathrm{d}\chi\, \chi\, q(\chi)}{a(\chi)} \delta(\chi\theta, \chi) \tag{5}$$

in a flat Universe. Here H_0 is the current Hubble parameter, Ω_m is the current matter density in units of the critical density, a is the scale factor, δ is the matter overdensity, χ is the comoving distance, and the lens efficiency q is defined as

$$q(\chi) = \int_\chi^\infty \mathrm{d}\chi'\, n(\chi') \frac{\chi' - \chi}{\chi'} \tag{6}$$

in terms of the source distribution $n(\chi')$. The line-of-sight projection in the expression for κ indicates why the most interesting weak lensing measurements involve binning by source redshift ("tomography"): instead of averaging over all line-of-sight structure, using a set of distinct redshift bins enables measurement of how cosmic structure has grown with time.

From the initial detections of cosmic shear (Bacon, Refregier & Ellis 2000; Van Waerbeke et al. 2000; Wittman et al. 2000; Rhodes, Refregier & Groth 2001) to recent measurements (e.g., Becker et al. 2016; Jee et al. 2016; Hildebrandt et al. 2017; Troxel et al. 2017), there has been substantial evolution of methodology to ensure that either observational or astrophysical systematic errors do not dominate the measurements. Currently, three weak lensing surveys are ongoing: the Kilo-Degree Survey (KiDS; de Jong et al. 2013), the Dark Energy Survey (DES; Dark Energy Survey Collaboration et al. 2016), and the Hyper Suprime-Cam survey (HSC; Aihara et al. 2017). In the 2020s, several "Stage-IV" (Albrecht et al. 2006) surveys will further increase the precision of these measurements: Euclid (Laureijs et al. 2011), LSST (LSST Science Collaboration et al. 2009), and WFIRST (Spergel et al. 2015).

The focus of this review is on weak lensing method development and systematics mitigation in preparation for the surveys that will happen in the 2020s, which will have such small statistical errors that serious discrimination among dark energy models will be possible, the era of "precision cosmology" (Figure 2, left panel). Since the weak lensing shear is so small compared to the intrinsic, randomly-oriented galaxy ellipticities (often called "shape noise"), averaging over very large ensembles of galaxies is the key to achieving small statistical errors. Indeed, this shape noise dominates over the impact of pixel noise in galaxy shape estimation for nearly all galaxies above detection significance of $\sim$5. Hence weak lensing measurements generally use galaxies that are as faint and small as possible, down to the limit imposed by the need to control systematic uncertainties. I describe the obstacles in the path towards a statistical error-dominated analysis, status of existing analysis methods, and areas where more work is needed. How do we do weak lensing correctly
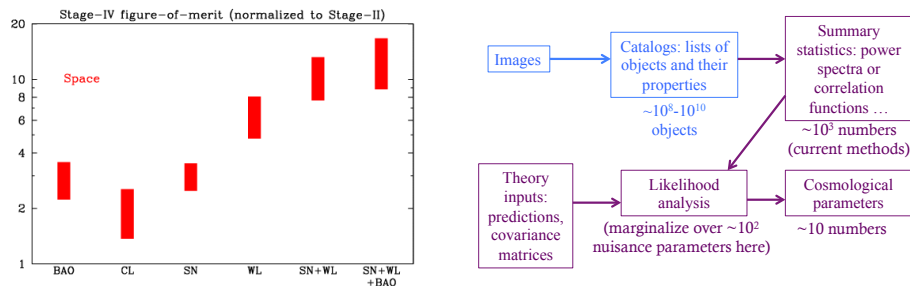
Figure 2: **Left:** Forecast of dark energy constraining power in Stage-IV space-based surveys of the 2020s, normalized with respect to the Stage-II surveys that existed in ∼2005 (from Albrecht et al. 2006). The increase in this figure-of-merit is based on the ability to constrain the equation of state of dark energy, including its time evolution, for baryon acoustic oscillations (BAO), galaxy clusters (CL), Type Ia supernovae (SN), weak lensing (WL), and two probe combinations. While the exact details for actual Stage IV surveys will depend on the survey design, this figure nonetheless demonstrates the basic principle that has driven much of the excitement about weak lensing in the cosmological community. **Right:** Basic outline of the weak lensing analysis process, where the blue and dark purple respectively indicate the parts of the analysis covered in Sections 2 and 3 of this review.

when we need to trust it for potentially novel results, such as unusual findings about dark energy? The goal of the review is to explain the technical state of the art and challenges moving forward towards this goal.

This review will cover both observational and theoretical systematics in weak lensing two-point correlations, both shear-shear (cosmic shear) and shear-galaxy ("galaxy-galaxy lensing"). The canonical cosmological weak lensing analysis from Stage IV surveys will include joint analysis of shear-shear, shear-galaxy, and galaxy-galaxy correlations; however, I refer the reader to other works for thorough discussion of systematics in galaxy-galaxy correlations (e.g., Morrison & Hildebrandt 2015). Throughout this work, I refer to two-point correlations generically; in practice, they may be estimated in configuration space ("correlation functions") or Fourier space ("power spectra"). The review will cover the entire path from raw images to science; see analysis flowchart in the right panel of Figure 2. It will focus on cosmological distance scales, and will not cover the possibility of using small-scale lensing and clustering (e.g., More et al. 2015), which brings in a host of additional theoretical and observational issues, or cluster number counts (e.g., Hoekstra et al. 2015).

To enable thorough discussion of the above topics, several other approaches to weak lensing analysis will be neglected. These include shear beyond two-point correlations; flexion; lensing magnification; lensing cosmography (constraints on distance ratios rather than structure growth); and weak lensing outside of the optical or NIR wavelength range, such as radio lensing. Lensing of the Cosmic Microwave Background (CMB; e.g., Planck Collaboration et al. 2014) will be discussed as a consistency check on optical lensing, without coverage of its systematic uncertainties.

The structure of this review is as follows. I divide the weak lensing analysis process into two major steps: from images to catalogs with measured object properties (Section 2), and from catalogs to cosmological parameters (Section 3). The additional step of detecting
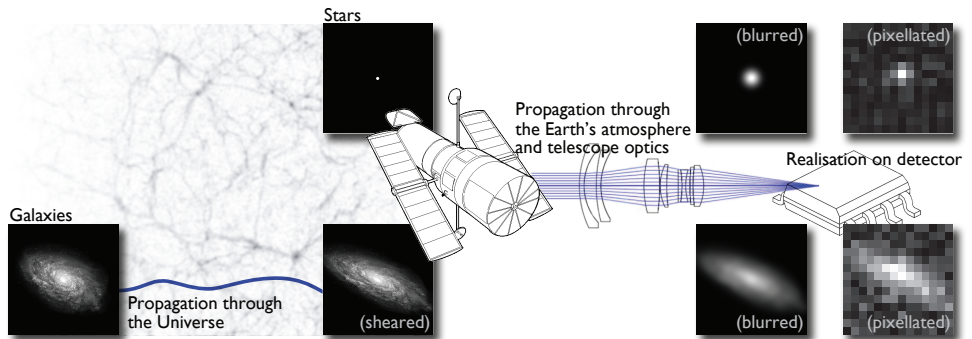
Figure 3: An illustration of the processes that affect the galaxy image (from Mandelbaum et al. 2014), including lensing followed by other effects that also cause coherent shape distortions, such as convolution with the point-spread function (or PSF) due to the atmosphere (for ground-based telescopes) and telescope optics.

and controlling for observational systematics more generally is described in Section 4. I summarize the future prospects for the field in Section 5.

2. FROM IMAGES TO CATALOGS

The full weak lensing analysis process goes all the way from the raw pixel data to cosmological parameter constraints. While somewhat artificial, it is common to separately consider the analysis steps from images to catalogs, followed by catalogs to science. This division partly reflects where certain systematics can be mitigated. Systematics related to the measurement process have a first-pass correction during the "images to catalogs" pipeline, and any mitigation for insufficiency of those corrections occurs in the "catalogs to science" pipeline. Theoretical systematics, i.e., those related to our insufficient knowledge of astrophysics, can only be mitigated in that second step. Hence we can think of the "images to catalogs" pipeline as the place where the weak lensing community attempts to estimate the properties of astronomical objects as accurately as possible, and the "catalogs to science" pipeline as the place where all residual systematics must get mitigated.

This section focuses on the first part of that pipeline. The basic challenge of inferring the lensing shear from galaxy images is illustrated in Figure 3. I will describe the nature of the challenges that arise at each step, the state of the art, and directions for future work.

2.1. PSF modeling

In this review, I consider the atmospheric PSF, optical PSF, pixel response, and charge diffusion together as the effective PSF. In other words, the model is that the pixel response (ideally a top-hat function, though reality can be more complex, resulting in higher-order corrections) is convolved with the other PSF components, and then the image is sampled at pixel centers[1].

---

[1]This model is violated if the pixels do not form a regular grid; current estimates suggest that the impact of deviations from a regular grid in real sensors are sufficiently small to ignore even for
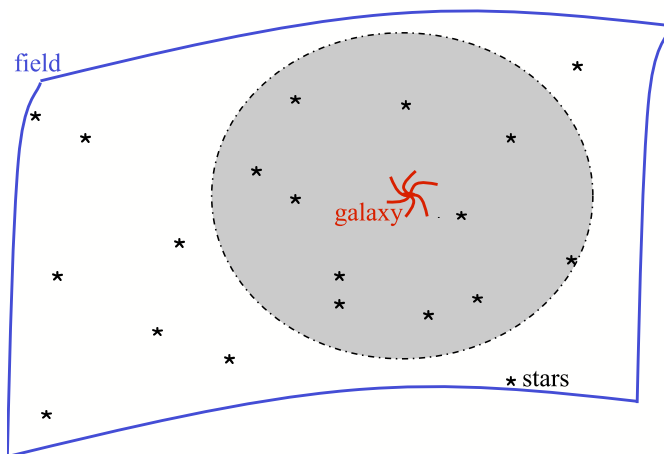
Figure 4: An illustration of the PSF interpolation problem (credit: Paulin-Henriksson et al. 2008, A&A, 484, 67, reproduced with permission © ESO). From a sparse sampling of stars in a given field, the PSF must be interpolated to the positions of galaxies so their properties can be measured.

Inferring coherent weak lensing distortions requires correction for the effect of the PSF, which if insufficiently corrected (a) dilutes the shear estimates, causing a multiplicative bias that is worse for small galaxies, and (b) imprints coherent additive corrections to the galaxy ellipticity values, due to the PSF anisotropies. Methods for removing the impact of the PSF from shear estimates all come with the assumption that the PSF is known. Hence, modeling the PSF correctly is an important challenge for weak lensing; errors in PSF model size and shape result in multiplicative and additive shear biases, respectively. The exact impact on the ensemble weak lensing shear observables depends not just on mean PSF size or shape errors, but rather their spatial correlations, and the distribution of galaxy properties. The formalism for understanding these effects either through simulations or through a moments-based formalism for propagating PSF modeling errors into shear biases was developed over the past decade (Hoekstra 2004; Hirata et al. 2004; Jain, Jarvis & Bernstein 2006; Paulin-Henriksson et al. 2008; Rowe 2010). While accurate determination of the PSF model is critical for weak lensing cosmology, it is fortunately a systematic uncertainty that comes with null tests that can be used to empirically identify problems, drive algorithmic development, and derive bias corrections.

In principle, the PSF modeling process may be thought of as having two components (see Figure 4). The first is using bright star images to model the PSF. The second is interpolating to other positions so the PSF model can be used to measure galaxy photometry and shapes (for discussion of several PSF interpolation methods, see e.g. Bergé et al. 2012; Gentile, Courbin & Meylan 2013; Kitching et al. 2013; Lu et al. 2017). Challenges in PSF modeling
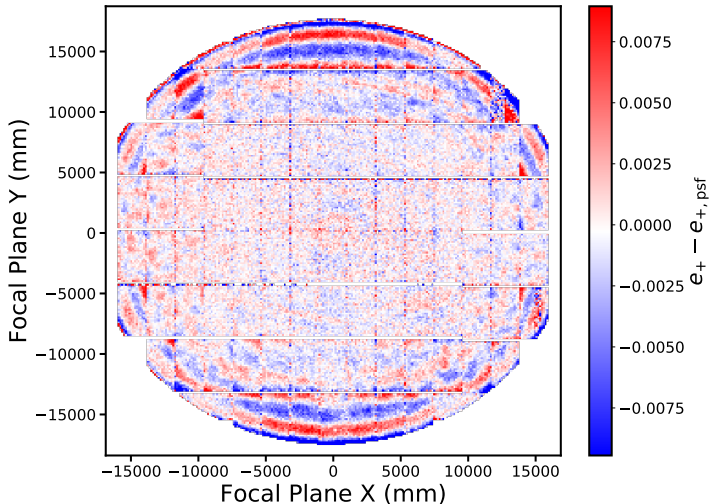
LSST (Baumer, Davis & Roodman 2017)

Figure 5: The color scale shows the PSF model radial ellipticity residual (Δe_+) averaged over many HSC survey exposures. Here 'radial' refers to the ellipticity component defined with respect to the focal plane center. The rings of nonzero values indicate a coherent misestimation of the radial ellipticity of the PSF near the focal plane edge edge. Figure provided by Bob Armstrong, based on figures and data from Bosch et al. 2017.

and interpolation differ for ground- and space-based imaging. The optical PSF can be thought of as varying slowly over the field-of-view and exhibiting a limited set of predictable patterns, which is one of the appeals of space-based weak lensing measurements. In contrast, the atmospheric PSF exhibits stochastic behavior (for which the power spectrum can be measured, and each exposure is a different realization of that power spectrum).

Some PSF modeling and interpolation methods are purely empirical. These involve choosing a set of basis functions to describe the bright star images, and some functions for interpolating between those images within a single CCD chip (e.g., regular or Cheby-shev polynomials, though more sophisticated options exist). The PSF tends to exhibit discontinuities at chip boundaries due to slight inconsistencies in chip heights, which makes modeling purely within chips a common process. An example of an empirical PSF modeling algorithm is PSFEx (Bertin 2011), which was used for both DES and HSC. Figure 5 shows a typical failure mode for empirical approaches: failure to properly describe PSF variations in parts of the focal plane with the adopted interpolation functions.

One method that has the potential to address both the PSF modeling and interpolation problems is Principal Component Analysis, or PCA (Jee et al. 2007; Schrabback et al. 2010). The PCA method considers all of the survey data, and identifies the most important patterns in PSF model variation across that data. PCA analysis can be done at the level of PSF images or any compact representation of the PSF, such as its second moments. Due to its use of all survey data, with stars in different exposures sampling different locations in the focal plane, the method can determine PSF model variation as a function of focal plane position at higher spatial frequency than is possible using only the stars observed on

a single exposure. Naively, this is a more promising method for space-based data (which only has an optical PSF determined by a relatively limited set of physical parameters).

Another approach to PSF modeling is a physics-based forward-modeling approach. One past example of this (for the *Hubble Space Telescope*, or *HST*) is ray-tracing through a physical model of the telescope optics using `Tiny Tim`[2]. This was used by the COSMOS team (e.g., Leauthaud et al. 2007) for several of its analyses. The idea is to forward-simulate the PSF as a function of position in the focal plane in each band given a limited set of physical parameters such as variation in focus position, then match the stars in each exposure against those models to identify the best model for each exposure. The PSF model interpolation then uses the finely-spaced grid of models rather than the more widely-spaced stars. The most obvious failure mode for forward-modeling of the PSF is if some relevant physics determining the PSF is not included in the model (for an example of this in practice, see Sirianni et al. 1998).

While physical modeling seems most appropriate for space-based PSF modeling and interpolation, in principle one approach for LSST is a combination of an optical model (perhaps with additional empirical constraints from wavefront data, e.g. Roodman, Reil & Davis 2014 and Xin et al. 2016) and a stochastic atmospheric PSF model using, for example, Gaussian processes or a maximum entropy algorithm (Chang et al. 2012). Empirical modeling of the optical PSF using wavefront measurements from out-of-focus exposures at least partially mitigates the concern about missing physics in the pure forward-modeling approach. One important advantage of combined optical plus atmospheric PSF modeling is that the optical component can potentially include the chip discontinuities, enabling the atmospheric model to use the entire focal plane rather than modeling each chip separately.

Recently, work on PSF modeling systematics has gone beyond second moments-based size and shape estimates. Getting higher order moments of the PSF model wrong may be problematic; such errors can be identified most easily by comparing stacked star images and PSF models to identify differences that are not easily described using the second moments. Quantifying their impact on weak lensing is most easily done with simulations; no simple analytic formalism has been worked out in this case. Also, failure of the PSF and galaxy profiles to be well-approximated by a Gaussian (e.g., like space-based PSFs, since the Airy function has a formally infinite variance) causes the simple analytic formalism for second moments to fail, rendering simulations necessary.

Another effect that has gotten more attention in recent years is the chromatic PSF. Both the atmospheric and optical PSFs depend on wavelength; even the sensor contribution to the PSF can exhibit slight wavelength dependence as well (Meyers & Burchat 2015a). Within a single broad photometric band, the effective PSF for any given object must depend on its spectral energy distribution (SED). Since stars and galaxies tend to have different SEDs, they will have different effective PSFs, which is a problem when using star images to infer the PSF for galaxies. Even worse, galaxy color gradients cause a violation of the assumption that there is a single well-defined PSF for the galaxy. Substantial work has been done on the chromatic PSF effect on weak lensing measurements (Cypriano et al. 2010; Plazas & Bernstein 2012; Voigt et al. 2012; Meyers & Burchat 2015b; Er et al. 2017). While the magnitude of the effect tends to be larger for space-based PSFs, for which the relevant physics scales like λ rather than $\sim \lambda^{-1/5}$ for atmospheric PSFs, the actual importance of the effect for science depends on the requirements on how well PSF size is known. These

---

[2]http://www.stsci.edu/software/tinytim/

requirements may be stricter for ground-based surveys given their larger PSF size. Broader bands, such as those planned for the Euclid survey, are more problematic in this regard. The above references include work on mitigation schemes that approach the level of systematics control needed for future surveys.

As mentioned above, there are well-defined null tests that can directly reveal PSF modeling errors, unlike some of the other systematic uncertainties described in this review. These null tests typically involve sets of stars (high-significance detections) that were not used for PSF modeling. A comparison of their sizes and shapes based on second moments with the PSF model sizes and shapes at the positions of those stars can be quite revealing. While the most obvious thing to do is make a histogram of those differences and look for systematic biases, the spatial correlation function of these errors determines how weak lensing observables will be biased due to PSF modeling errors. For PSF shape errors, there are five relevant correlation functions (called ρ statistics), two introduced by Rowe (2010) and three by Jarvis et al. (2016); these include factors of the PSF shape residuals, the PSF shape itself, and the PSF size residuals, and directly correspond to additive terms in the shear-shear correlation function generated by PSF modeling errors. For examples of their use in real survey data, see Jarvis et al. (2016); Mandelbaum et al. (2017b).

An additional diagnostic is to compare the distribution of PSF shape and size errors for the non-PSF star sample with the distribution for those stars used to estimate the PSF. If the two samples have the same detection significance, then the widths of the distributions can reveal whether there are overall PSF modeling issues (similar breadth of the distributions) or whether there may be issues with overfitting or interpolation (broader distribution for non-PSF stars). Comparison of the ρ statistics computed with PSF and non-PSF stars can also be revealing. Finally, stacking the PSF size or shape residuals in the focal plane coordinate system, across multiple exposures, can reveal systematic failure to model recurring optical features in the PSF; see Figure 5 for an example.

Aside from the obvious approach of developing more sophisticated PSF modeling algorithms, survey strategy may mitigate the impact of single-exposure PSF modeling errors on the final multi-exposure shear estimate. For example, consider the not atypical case that PSF modeling errors systematically correlate with distance from the center of the focal plane (e.g., Figure 5). If all exposures in that region have very small dithers, then each galaxy will be observed at nearly the same focal plane position in all exposures, and their PSF modeling errors will be coherent. If there is substantial dithering compared to the size of the focal plane, then the galaxy will be observed at many different focal plane positions, and the systematics due to PSF modeling errors will average down. Depending on the coherent structure of PSF modeling errors, rotational dithering may also be beneficial. Using survey strategy to reduce systematics in large-scale structure statistics was considered by Awan et al. (2016) for LSST, where hundreds of exposures make this approach to systematics mitigation possible (LSST Science Collaboration et al. 2017), but a similar study in the weak lensing context has not yet been performed.

2.2. Detector systematics

For the purpose of weak lensing, detector non-idealities can cause two problematic types of systematics that cannot be treated as a simple convolution (and hence as part of the PSF). First, there are flux-dependent effects that predominantly affect bright objects, such as nonlinearity or the brighter-fatter effect discussed below. Since weak lensing measure-

ments are dominated by faint galaxies, but the PSF for those faint galaxies is estimated via interpolation between the PSF modeled from bright stars, detector non-idealities affecting bright objects result in the wrong PSF being used when estimating shear from the faint galaxies[3]. The second type of detector non-idealities affect all objects, due to defects that correlate with position or galaxy orientation on the detector. They can induce spurious coherent shear signals or photometry errors, and/or cause selection biases due to coherent masking patterns. While correction for some detector non-idealities such as nonlinear response has long been taken for granted as happening before the stage that weak lensers care about, the field's approach to detector systematics has otherwise been varied.

For example, the detectors on the *HST* are known to suffer from charge transfer inefficiency (CTI) due to radiation damage. CTI imparts a preferential direction in the images, which is a problem for weak lensing measurements, the goal of which is to identify coherent smearing in galaxy shapes. A physically-motivated pixel-level correction scheme was pioneered primarily by and for weak lensers, resulting in a 97% correction for this effect (Massey et al. 2010; Rhodes et al. 2010).

In the past few years, there have been many more studies on the detailed impact of detector non-idealities on weak lensing. One example is the so-called "brighter-fatter" effect (Antilogus et al. 2014; Guyonnet et al. 2015), wherein brighter objects spuriously appear slightly broader than fainter ones due to the electric field sourced by charges accumulated within a pixel deflecting later light-induced charges away from that pixel. Conceptually, one can think of this effect as a dynamic change in pixel boundaries. While early work proposed methods for estimating the effect using flat fields, later work has focused on detailed simulation and measurement methods (e.g., Lage, Bradshaw & Tyson 2017). This effect is quite problematic for weak lensing because the if left uncorrected, the PSF inferred from bright stars is not the relevant one to use when removing the impact of the PSF on the faint galaxies that dominate weak lensing measurements. Fortunately, empirical tests of PSF model fidelity can be carried out as a function of magnitude to confirm that the brighter-fatter effect has been corrected at the necessary level. These were used in the HSC survey to identify the impact of the brighter-fatter effect, and show that the corrections were sufficient for weak lensing science in HSC (Mandelbaum et al. 2017b).

The conceptual framework mentioned above, wherein some detector non-idealities are thought of as dynamically adjusting pixel boundaries and therefore pixel sizes (resulting in astrometric and photometric errors), applies to several other detector effects. For example, the concentric rings known as "tree rings" and bright stripes near detector edges known as "edge distortions" in DES can be modeled this way. Plazas, Bernstein & Sheldon (2014) proposed that the templates for these effects derived using flat-field images can be used in the derivation of photometric and astrometric solutions. In other words, the WCS (world coordinate system) that maps from image to world coordinates can include these (admittedly rather complex) effects (Rasmussen et al. 2014; Baumer, Davis & Roodman 2017; Bernstein et al. 2017a). Note that modeling the effect as part of the WCS is a distinct solution from pixel-level correction, such as was used for CTI; the WCS-based correction kicks in when measuring positions, photometric quantities, and galaxy shapes from the images. It is a valid approach in the limit that the detector effect can be described with a WCS that varies slowly compare to the size of a pixel, though since it is common practice to take the

---

[3]Technically, without correction for the brighter-fatter effect, the PSF estimated from the bright stars is not even the right PSF to use for the bright galaxies.

local affine approximation of the WCS when measuring individual objects, that imposes a more stringent constraint that the WCS can be considered locally affine over the scale of individual objects.

The details of detector non-idealities depend on the detectors used for each survey (though common mitigation schemes can be used for conceptually similar systematics in multiple surveys). The general framework for how detector effects impact weak lensing developed in Massey et al. (2013) for Euclid would be relevant for other surveys, with the exact effects to be considered varying. A new complication is the fact that WFIRST will use near-infrared (NIR) detectors, which operate differently from CCDs. CMOS devices have 1 readout path per pixel, whereas CCDs have 1 readout path per channel; calibrating all pixels to within requirements, including the effect of cross-talk, is more challenging for CMOS devices. The use of different types of detectors necessitates studies of the impact of various NIR detector effects, some of which are present in CCDs (e.g., nonlinearity and brighter-fatter: Plazas et al. 2016, 2017), and others that are not, such as interpixel capacitance (IPC: Kannawadi et al. 2016), persistence, and correlated read noise. Further work on characterizing the impact of NIR detector systematics for weak lensing is underway, with an eye towards placing requirements on hardware and survey strategy to ensure that residual systematics can be mitigated at the level needed for weak lensing with WFIRST.

A range of correction schemes have been discussed for various detector effects, including pixel-level correction, including them in the WCS, and applying catalog- or higher-level mitigation schemes such as template marginalization. Understanding the spatial- and time-dependence of detector effects is also quite important, and can be a challenge especially for CMOS detectors. In principle there may also be the option of indirect mitigation through survey strategy for effects that correlate with location on the focal plane (e.g., following the approach of Awan et al. 2016). Additional work is needed to quantify the impact of various low-level detector systematics for upcoming surveys, including lab measurements and simulations of their impact on weak lensing. Detectors are sufficiently complex, and requirements on systematics sufficiently strict for upcoming surveys, that analysis of realistic lab data is a necessity to avoid unpleasant surprises during commissioning – with ongoing efforts in both WFIRST and LSST (e.g., Seshadri et al. 2013; Tyson et al. 2014).

2.3. Detection and deblending

Traditionally, object detection is carried out by detecting peaks above some detection threshold. For weak lensing, additional cuts are typically placed to identify objects that can be well-measured; these cuts can be a source of "selection bias" (see Section 2.5).

"Deblending", the process of removing the influence of light from other objects above that same detection threshold, requires the identification of detections that have multiple peaks. This naturally leads to two regimes: recognized blending, wherein the multiple peaks are recognizable, and unrecognized[4] blending, wherein the deblending algorithm is not triggered because multiple peaks are not identified within the detection (see Figure 6). The same system could switch between these categories depending on the PSF size. In the case of mild blending, one can ask whether the deblending algorithm results in unbiased measurements of object properties, or whether there are coherent systematics requiring mitigation and/or removal of mildly blended objects. For unrecognized blends, the only possibility is

---

[4]Terminology for these varies; e.g., they are called "ambiguous" blends in Dawson et al. (2016).
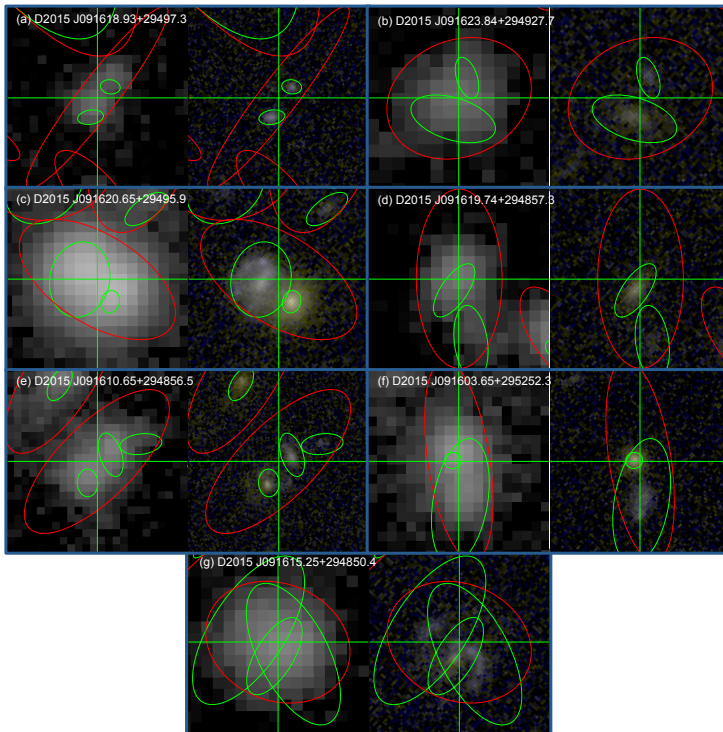
Figure 6: An illustration of the issues with unrecognized blends (© AAS. Reproduced with permission, from Dawson et al. 2016). Each pair of images shows a ground-based (left) and space-based (right) image of the same system, with the shapes of the galaxy detection in the ground-based and space-based images shown as red and green ellipses.

to quantify their rate of occurrence, and apply analysis-level mitigation strategies.

For weak lensing, the primary concerns are the impact of blending on shear and photometric redshifts. If we consider unrecognized blends, then two objects at the same redshift should have the same shear, and therefore it should be possible to properly calibrate shear estimates for the combined (non-deblended) object. However, for photometric redshifts of unrecognized blends at the same redshift, the situation is only simple if the two objects have the same spectral energy distribution (SED). If they do not, then the composite object will correspond to some possibly strange SED, which may not give a correct photo-z. If the objects are at different redshifts, it is unclear how the shear estimate should be interpreted (though the case of large flux ratios or small redshift differences is simpler than the completely general case). The photometric redshift estimation is also complexified by the superposition of SEDs at different redshifts, even for reasonably large flux ratios. Unfortunately, the majority of unrecognized blends will be at different redshifts (Kirkby et al. *in prep.*), except perhaps in the centers of galaxy clusters.

The weak lensing community has recently come to confront the issue of blends more directly; this area requires more work, both on the deblending algorithms and the post-deblender systematics quantification and mitigation. In the past, it was common practice to

eliminate galaxies recognized as having nearby neighbors; e.g., this was done in CFHTLenS[5] (Miller et al. 2013). That approach does not help with unrecognized blends, and can give a few-percent scale-dependent bias in shear-shear correlations due to the fact that close pairs are more prevalent in high-density regions (Hartlap et al. 2011) unless a weighting scheme is used to mitigate that effect. The early Dark Energy Survey Science Verification results imposed cuts on recognized blends (Jarvis et al. 2016) and ignored the issue of unrecognized blends (while leaving a 5% uncertainty on the multiplicative bias to cover this or other uncorrected issues). Their Year 1 (Y1) results included a more sophisticated multi-object fitting strategy, with a careful study of the impact of blending using simulations (Samuroff et al. 2017). In the HSC survey, which is deeper, Bosch et al. (2017) notes that 58% of the objects detected in the HSC Wide survey are recognized blends. As a result, rejecting blended objects is not a viable strategy, and estimation and removal of blend-related systematics is necessary from the outset[6]. This was done using simulations that included a realistic level of nearby structure around galaxies (Mandelbaum et al. 2017a).

For future surveys such as LSST, removing blended objects will not be a viable strategy due to both their prevalence and the fact that a truly non-negligible fraction of them are unrecognized. Dawson et al. (2016) quantified the unrecognized blend population as exceeding 10% for a survey like LSST, and investigated differences in its intrinsic ellipticity distribution, which is relevant for weak lensing cosmology. Chang et al. (2013) included blending when quantifying the expected galaxy source number density and redshift distribution from LSST, and estimated the impact of rejecting those blend systems recognized as seriously blended. They note that the need to reject these objects depends on our ability to quantify and remove blending systematics (and that the threshold for "seriously" blended depends on the deblending and measurement algorithms).

The combination of space-based imaging from Euclid and/or WFIRST with LSST ground-based images has the potential to benefit LSST on this issue (e.g., Jain et al. 2015 and Rhodes et al. *in prep.*). One could imagine a separate round of joint pixel-level analysis resulting in forced deblending for LSST based on higher-resolution space-based imaging. In the area of overlap between those surveys, the space-based data can substantially aid in deblending mildly blended cases and in detecting a larger number of otherwise unrecognized blends. It can also be used to learn about the impact of blending for LSST alone, and develop systematic error budgets for the entire LSST survey region.

More work is clearly needed to develop a framework for quantifying systematics in shear inference and photometric redshifts due to both recognized and unrecognized blends for both ground- and space-based surveys. The impact of blending on photometric redshift estimation and inference of the correct redshift distribution for photometric redshift-selected samples is particularly tricky, since the spectroscopic redshift selection and failure rate for samples used for training and calibrating photometric redshifts may result in them having different unrecognized blend rates than the general galaxy population. Both improved deblenders and systematics mitigation schemes would be beneficial. For all surveys, algorithms that include color and other information in new ways will likely be explored in

---

[5]More specifically, galaxies with overlapping isophotes were rejected, while those that did not overlap very strongly and for which one galaxy could be masked without too much influence on the fit results for the other galaxy were retained.

[6]A cut on the "blendedness" parameter in Mandelbaum et al. (2017b) removes a very small fraction of objects, of order 1%, that were dominated by spurious detections near very bright objects. It does not affect the much larger fraction of genuinely blended real galaxy detections.

the coming years (e.g., Joseph, Courbin & Starck 2016); another example is the secondary deblender used in crowded cluster regions for DES (Zhang et al. 2015). Unfortunately, well-established algorithms for crowded stellar fields (e.g., Stetson 1987) are not relevant in this situation, and more algorithm development is needed for the complex multi-galaxy and star-galaxy blend systems that will dominate surveys like LSST.

2.4. Image combination

Nearly all surveys used for weak lensing science have multiple images at each point that must be combined to reach the full survey depth. Taking multiple exposures can be helpful to prevent excessive build-up of artifacts like cosmic rays or saturated stars on any one image, to fill in the gaps between CCD boundaries or artifacts, and to build a Nyquist-sampled image out of multiple undersampled images. The manner in which image combination is done is important for weak lensing science. The primary consideration that determines the available algorithms is whether the imaging is Nyquist sampled or not, which is primarily a difference for ground vs. space-based imaging. For space-based imaging, the primary concern during the image combination stage is how to properly reconstruct a Nyquist-sampled image, while for ground-based imaging, the individual images are Nyquist sampled, and the main question is how to optimally combine information across exposures.

Most space-based instruments are (by design) not Nyquist sampled, but a wise choice of dithering strategies enables reconstruction of a Nyquist-sampled image. The need to reconstruct a Nyquist-sampled image from multiple undersampled images should factor into survey strategy for space-based weak lensing surveys; e.g., the expected rate of cosmic rays should be factored into the calculation of how many exposures are needed at each point (to allow for periodic losses and still obtain a Nyquist-sampled image). The first principled method for combination of space-based telescope images was presented in Lauer (1999). This method used linear algebra to solve out the aliased Fourier modes given some sub-pixel dither pattern, and reconstruct a Nyquist-sampled image. Rowe, Hirata & Rhodes (2011) generalized this approach to address several challenges: the fact that when dither patterns are comparable to the side of individual chips, the different exposures at each point will experience different field distortions; the ability to handle holes due to, e.g., cosmic rays; and the fact that the input PSFs for the different exposures may differ. Their method, IMCOM[7], has not yet been used for survey data, but it may be the best approach to use for surveys like WFIRST. The commonly used MultiDrizzle method (Fruchter & Hook 2002) carries out interpolation on the individual non-Nyquist-sampled exposures. This problematic method necessarily causes stochastic aliasing of the PSF (Rhodes et al. 2007), which means that aliased modes are not fully removed, and the PSF of the resulting coadded image may not even be constant across a galaxy image. Later updates to the MultiDrizzle method were designed to eliminate these high-frequency artifacts and convolution with an interpolant kernel (Fruchter 2011). Finally, multi-epoch model fitting is a valid approach to image combination for undersampled data, and in some sense may be the most optimal approach, provided that a good per-image PSF model is known. Further investigation on this point is needed to weigh the tradeoffs between these options.

For ground-based imaging, there are multiple image combination options. The first is to use a coadded image for all science, including PSF estimation. Several challenges make this

---

[7]https://github.com/barnabytprowe/imcom

approach sub-optimal. These include the fact that depending on how coaddition is carried out, the coadd may not even have a well-defined PSF at each point (for example, inverse variance weighting that depends on the total flux, or use of a median for the coadd). The answer to this challenge is to generate the coadd in a principled way that results in a single well-defined PSF at each point (e.g., Bosch et al. 2017). The primary remaining systematic challenge for this method is that the PSF changes discontinuously wherever there is a chip edge in any exposure contributing to the coadd at a given point. Given the typical stellar density in images used for weak lensing, it is very difficult to model these small-scale changes in PSF. There is an additional concern with respect to statistical errors, since coaddition may effectively discard information that is present in the best-seeing images.

The second option is to use a coadded image for measurements of object properties, but produce the coadded PSF based on the appropriate weighted combination of the single-exposure PSF models. This "stack-fit" approach was used for the DLS and HSC surveys (Jee et al. 2013; Bosch et al. 2017). It enables the elimination of the primary systematics concern with the first approach mentioned above (estimation of the coadd PSF), while retaining concerns such as information loss from the best-seeing exposures. There are also lower level concerns about relative astrometry, which can behave like a blurring kernel in the coadded image. If the relative astrometric errors are well-characterized, they can be accounted for by including this blurring in the coadded PSF, though in the HSC survey this was not necessary because the astrometric errors were sufficiently small as to have a negligible effect on weak lensing (Mandelbaum et al. 2017b). While modeling the PSF discontinuities is not a problem with this approach, it is still the case that some fraction of objects will be lost due to their being so close to the edge of a sensor in some exposure that the PSF cannot be modeled as effectively constant across them. This issue is more important as the number of contributing exposures in the coadd increases.

Finally, it is possible to use a coadd for object detection and deblending, while measuring shear and (optionally) galaxy photometry through simultaneous fitting to the individual exposures. This approach was proposed for LSST (Tyson et al. 2008), and used for DES Y1 (Zuntz et al. 2017), CFHTLenS (Miller et al. 2013), and KiDS. In principle, this allows for marginalization over the centroid positions in the individual exposures, which was used in CFHTLenS to marginalize over relative astrometric errors. Additional benefits include the fact that the information in the best-seeing images can be preserved. There are several limitations to this approach. First, some measurement methods (such as those based on measurement of moments) do not map to a combined likelihood framework and therefore cannot be used in a simultaneous fitting approach. Second, this approach is computationally intensive. When producing a best-fitting model, with M iterations, fitting to a coadd requires M model convolutions with the PSF, while fitting to N individual exposures with different PSFs requires $N \times M$ model convolutions. For LSST, which will have hundreds of exposures per object in the final dataset, this will require clever optimization to reduce computational expense. Alternatively, use of a fully Bayesian shear estimation method (e.g., Bernstein et al. 2016) that includes computation only of moments on each exposure would be a less expensive way to combine information from all exposures; in this case, the complexity is moved into the later shear inference step, and will not scale linearly with N.

Several ideas have been proposed to optimize the simultaneous fitting approach so that it is more feasible for future surveys. First, as in one of the methods used in DES (Sheldon 2015), representing the galaxy and PSF models as sums of Gaussians with different scale radii can drastically speed up the calculations. This could be done to produce an initial guess

at model parameters before switching to a model with full complexity. Or it could be done in combination with a technique like metacalibration, which will soak up the error induced by model simplification in its estimate of the shear response (see Section 2.7 for a discussion of metacalibration). Second, it would be possible to fit for object properties using a coadd to get an initial guess, and then tweak that model using fits to individual exposures. Third, it may be possible to use some hybrid of the simultaneous fitting and coadd approaches. For example, if the LSST exposures were split into 10 sets based on percentiles in the PSF size, and each of those sets were coadded, then they could be used for simultaneous fitting with very little loss of information in the best-seeing exposures. This would also alleviate the concern raised above with loss of objects falling on PSF discontinuities, since fewer exposures would contribute to each coadd. Further investigation into the interplay between information gain/loss and systematics for these approaches is needed in order to define a path forward for the field (Sheldon et al. *in prep.*).

Finally, as suggested above, there is some connection between methods used for image combination, deblending, photometry, PSF and shear estimation; the best solution for image combination may depend on what is being done for the other steps of the analysis process.

2.5. Selection bias

Selection bias arises when quantities used to select or weight the galaxies entering the lensing analysis depend on the galaxy shape. Usually this dependence is implicit rather than explicit, due to the details of image analysis algorithms or lensing magnification (which modifies sizes and brightnesses in a way that correlates with the shear). As a result, the probability of a galaxy entering the sample (or its assigned weight) depends on its alignment with respect to the shear or PSF anisotropy direction. This violates the assumption that galaxy intrinsic shapes are randomly oriented. If the selection probability depends on the shear, there will be a multiplicative bias, whereas if it depends on the PSF shape, there will be an additive bias.

In the case of continuous quantities used for selection (such as galaxy size) causing the bias, the bias is present only for galaxies near the boundary of the sample in the quantity used for selection. In contrast, while weights used to construct weighted averages are also continuous variables, biases related to the weighting scheme used to take ensemble averages (e.g., Fenech Conti et al. 2017) may be present throughout the sample. Finally, there are selection biases such as avoiding elongated structures (bad CCD columns) that can lead to selection bias depending on how they are imposed (Huff et al. 2014). Cuts on continuous quantities and on regions like bad columns are appropriate to avoid certain systematic errors, but if not applied with care, they can cause a selection bias.

There are several approaches to selection bias. One is to simply avoid it: define detection significances and apparent sizes compared to the PSF using round kernels, so that the results are insensitive to galaxy shapes (Jarvis et al. 2016). Another way is to estimate its magnitude through an analytic formalism based on moments (Hirata et al. 2004; Mandelbaum et al. 2005), and remove it. Its magnitude can be estimated using simulations and then removed, if the simulations include all physical effects that induce selection biases. For example, if the photometric redshifts are coupled to the galaxy shape then there could be a selection bias that can only be estimated using realistic multi-band simulations. Moreover, these estimation methods must take into account how selection bias varies based on the full range of observing conditions in the survey. Finally, self-calibration approaches to shear

estimation such as metacalibration (discussed in Sec. 2.7) offer the opportunity to directly estimate using only the real data, and remove selection bias.

Selection bias plays an important role in defining useful null tests (e.g., Mandelbaum et al. 2005; Jarvis et al. 2016). For example, it is commonly suggested that subsets of the galaxy sample should be used to carry out the lensing measurement, with the subsets giving consistent cosmology results in the absence of a systematic that depends on the quantity being used to divide the sample. However, the process of dividing up the sample can induce selection biases that are of order 5-10% depending on how this is done.

Until recently, selection biases have not attracted nearly the attention given to other shear biases (Sec. 2.7). In future, more work is needed to avoid selection biases from complex cuts related to galaxy blends, bad pixels, and other selection criteria that cannot be mitigated as straightforwardly as S/N or size.

2.6. Other aspects of the image processing

Several other steps in the image processing can affect weak lensing besides those explicitly called out in previous subsections. First, in order to detect and measure galaxy properties, the sky level must be estimated and subtracted. Errors in sky subtraction can cause coherent problems with object detection, photometry, and shear estimation near very bright objects – bright stars or collections of bright galaxies (e.g., in galaxy clusters). A spurious sky gradient can induce a spurious shear with respect to the location of the bright object causing the sky misestimation. This effect was identified and its impact on object detection, photometry, and shapes was quantified in the SDSS (Adelman-McCarthy et al. 2006; Aihara et al. 2011).

Another relevant issue is star-galaxy separation. There are two issues: the bright star sample used to estimate the PSF can be contaminated by galaxies; and the faint galaxy sample used to estimate lensing shear can be contaminated by (unsheared) stars. For current surveys, we have no evidence that star-galaxy separation algorithms are failing at problematic levels (e.g., in HSC, Bosch et al. 2017; Mandelbaum et al. 2017b). Given that more sophisticated methods for star/galaxy classification have been proposed, for example using machine learning, there is clearly room to improve to the level needed for upcoming surveys. Slightly more interesting issues with star-galaxy separation include binary stars contaminating the galaxy sample (Hildebrandt et al. 2017). In principle, these can be identified by looking for centroid offsets between different filters for highly elongated objects, for those binaries in which the stars have different SEDs.

The primary astrometric concern for weak lensing is the accuracy of the relative astrometry between different exposures for individual objects. The relative astrometry must be well-understood in order to fully understand the object measurements from simultaneous fitting and/or coaddition. Systematics due to errors in relative astrometry depend on exactly how the image combination is carried out; see Section 2.4. For an example of how astrometric calibration was carried out for the Dark Energy Survey, including correction for certain detector non-idealities (see Section 2.2), see Bernstein et al. (2017a) and Bernstein et al. (2017b). The astrometric calibration must include color terms to account for centroid shifts from differential chromatic refraction (DCR) and other low-level effects.

Finally, modeling of the noise in images is relevant to weak lensing measurements. Correlated pixel noise can arise due to low-level unresolved galaxies just below the detection threshold, methods used to combine multiple exposures into a coadd (Section 2.4), and pixel-level correction for effects such as CTI (Section 2.2). Since correlated noise means that

detection significances differ from the values one would naively assume given uncorrelated noise with the same variance, and shear biases depend on the detection significance (Gurvich & Mandelbaum 2016), it is important to understand the noise correlations.

2.7. Shear estimation

Since the initial detections of weak lensing shears around galaxy clusters in the 1990s, a large fraction of the weak lensing community's technical concern effort has focused on the challenge of correcting galaxy shapes for the impact of the PSF so they can be averaged to infer the lensing shear. In the past two decades, the field has moved from simple methods based on correcting second moments of galaxy images for the moments of the PSF (e.g., Kaiser, Squires & Broadhurst 1995), to a broader set of methods that include fitting parametric models (see methods described in Massey et al. 2007a), to greater conceptual sophistication in how shear should be inferred (see methods described in Mandelbaum et al. 2015). The community has set itself a series of blind challenges (Heymans et al. 2006a; Massey et al. 2007a; Bridle et al. 2009, 2010; Kitching et al. 2010, 2012; Mandelbaum et al. 2014, 2015) aimed at benchmarking the performance of shear estimation methods in a common setting, understanding the main challenges, and in the process developed an open-source, well-validated image simulation software package (GalSim[8]; Rowe et al. 2015).

It is important to note that we do not care about galaxy shapes. Indeed, the concept of a single number characterizing the galaxy shape is not well-defined in the presence of ellipticity gradients and irregular galaxy morphology. Given those real physical effects, the measured shape will depend on the radial weight function. Moreover, even for a galaxy with elliptical isophotes, shapes must be measured with weighted moments to reduce noise, and the measured shape will depend on the shape of the weight function. The assignment of "shapes" to individual galaxies is effectively the assignment of a single estimate of the local shear from each galaxy image, along with the assumption that the best ensemble estimator is the weighted mean of the point shear estimators. For this reason, comparison of galaxy shapes measured with different algorithms or in different surveys is rarely useful, and ensemble shear statistics provide the only meaningful comparison.

Shear systematics are often categorized into "multiplicative" or "additive" (in terms of what they do to ensemble shear statistics). Additive systematics can have quite different scale dependence from lensing shear correlations, depending on their physical origin. In Section 4 I discuss methods for empirically identifying additive bias. In contrast, multiplicative bias cannot be easily identified through null tests; typically simulations are required. While exact requirements vary depending on the details of the survey and the assumptions made about the weak lensing analysis, typically the upcoming Stage IV surveys require understanding of the shear calibration at the level of $\sim 2 \times 10^{-3}$ in order to avoid this systematic uncertainty dominating over the statistical uncertainties in the measurement. This is a factor of several smaller than the requirements for the measurements with the full areas of ongoing surveys, and includes all sources of multiplicative calibration uncertainties (e.g., PSF modeling errors), not just those due to the insufficiency of the PSF correction method.

The past five years have seen a shift in how the field approaches shear estimation. From the mid-1990s until $\sim$2011, the primary goal of weak lensers was to find ways to estimate per-object shapes that, when averaged together, provided an unbiased estimator

---

[8]https://github.com/GalSim-developers/GalSim

for the ensemble shear. During that time period, the typical magnitude of shear calibration biases decreased by a factor of a few. However, by that point it was becoming increasingly obvious that the "measure galaxy shapes and average them to get the shear" approach has fundamental flaws from a mathematical perspective. An example is noise bias, wherein the maximum-likelihood estimate of per-galaxy shapes at finite signal-to-noise is biased because noise changes the shape of the likelihood surface (Bernstein & Jarvis 2002; Hirata et al. 2004; Kacprzak et al. 2012; Melchior & Viola 2012; Refregier et al. 2012). Another example is model bias, which arises from the failure of model assumptions to describe real galaxy light profiles (e.g., Voigt & Bridle 2010; Melchior et al. 2010). Selection bias (Sec. 2.5) is another limitation of this approach.

Some proposed solutions for model and noise bias compete with each other: increasing model complexity may decrease model bias, while increasing noise bias due to the need to constrain additional degrees of freedom. Shear estimation methods based on measurements of per-galaxy shapes must balance these two considerations, with a finite amount of both biases in the ensemble shear estimates. Any method based on the use of second moments to estimate shears cannot be completely independent of the details of the galaxy light profiles, such as the overall galaxy morphology and presence of detailed substructure (Massey et al. 2007b; Bernstein 2010; Zhang & Komatsu 2011). Nor is noise bias avoidable: given the large intrinsic galaxy shape dispersion, lensing measurements must include galaxies down to relatively low signal-to-noise detections to achieve a reasonable overall signal-to-noise in the ensemble shear statistics.

Given the recent understanding of this situation, the community has sought other approaches to reliable ensemble shear estimation. There are four general classes of approach, some of which are compatible with each other.

Image simulations to estimate and remove calibration biases: Image simulations enable the estimation of biases in the shear signal due to the intrinsic limitations of the adopted shear estimation method. Given that shear biases depend on detailed galaxy morphologies (beyond second moments) and on the PSFs, there has been a move towards ever greater realism in the image simulations used by ongoing surveys (e.g., Zuntz et al. 2017). For example, several works have argued that one must include nearby structure around the galaxies in order to accurately predict shear biases due to nearby objects and unrecognized blends (Hoekstra et al. 2015; Hoekstra, Viola & Herbonnet 2017; Mandelbaum et al. 2017a), must account for variation of these biases with observing conditions across the survey, and have identified other key factors in image simulations for shear calibration. This approach will be challenging to take to the limit of future surveys, given our limited knowledge of galaxies, although the survey data itself provides a form of sanity check on the accuracy of the simulations and perhaps could enable an interative process to improve the simulations (see, e.g., the `sfit` method: Mandelbaum et al. 2015). To ensure that the statistical error on the derived bias corrections is a subdominant part of the overall error budget, it is necessary to simulate many more galaxies than exist in the survey itself. Moreover, use of calibrations as the sole way of estimating and removing shear biases does not provide an independent cross-check on the results (unlike, e.g., using one of the methods of calibrating the shear below, and then using simulations to validate that method as a cross-check).

Self-calibration: Recently, methods have been devised to calibrate ensemble shear statistics based on manipulations of the real images ("metacalibration": Huff & Mandelbaum 2017; Sheldon & Huff 2017). Metacalibration provides a way to determine the re-

sponse of an ensemble shear estimator for the real galaxy population in the data. This potentially enables direct removal of selection biases, depending on what stage of the image processing metacalibration is inserted into. The fact that it does not require assumptions about galaxy morphology is a clear virtue of this approach over image simulations.

CMB lensing: Since CMB lensing has very different observational systematics and a perfectly known source redshift, it is an attractive method for testing galaxy lensing (Vallinotto 2012; Das, Errard & Spergel 2013). Comparison of galaxy lensing with CMB lensing should not be thought of as a test of galaxy shear estimation, but rather of a combination of shear estimation and photometric redshift biases that both modify the lensing signal amplitude. When measuring cross-correlations between CMB and galaxy lensing, intrinsic alignments (Section 3.4) are a contaminant that must be modeled (Hall & Taylor 2014; Troxel & Ishak 2014; Chisari et al. 2015), unlike for correlations between the galaxy positions and CMB lensing. While current imaging and CMB surveys can only provide a $\sim 10\%$-level calibration (e.g., Baxter et al. 2016; Harnois-Déraps et al. 2016; Singh, Mandelbaum & Brownstein 2017), the situation will improve with future galaxy and CMB surveys (Abazajian et al. 2016). As demonstrated by Schaan et al. (2017) with forecasts that include systematic uncertainties, this method is unlikely to constrain the lensing signal amplitude at the level of precision needed to avoid a survey like LSST being systematics-dominated. However, it provides a valuable independent cross-check on the other methods of shear calibration in this list. Moreover, it may allow the shear calibration at high redshift to be constrained at the level needed for LSST, which is helpful because that is likely the regime with the most uncertainty on how to simulate the galaxy population.

Paradigm shift: The final approach described here, and perhaps the most principled one, is that since the meaning of per-galaxy shapes is questionable (given ellipticity gradients and other effects) and the approach of averaging them is fundamentally mathematically flawed, we should stop doing this. Instead, we should directly infer ensemble shear statistics in a way that avoids these assumptions, using the actual posterior shear estimate from each galaxy without assuming that an ellipticity is an unbiased proxy for it. Schneider et al. (2015) explored hierarchical inference of the shear, which involves parametric model fits that are then used to infer ensemble shear given a prior; this appeared promising, but requires further development due to the computational expense of the approach. Bernstein & Armstrong (2014) presented a Fourier-space Bayesian shear estimation method that does not involve averaging galaxy shapes, and should not be susceptible to either model or noise bias. This method involves measurements of moments in Fourier space for the galaxy sample to be used, and the construction of a prior for what the unlensed distribution of moments looks like using a deep subset of the same survey. Together, these can be used to infer the ensemble shears. The method was developed in subsequent work (Bernstein et al. 2016) to bring it closer to a practical shear estimator for use in real data, and the self-consistent modeling of photometric redshifts, selection biases, and measurements in multi-epoch data seems possible in principle. While work is needed to fully demonstrate the utility of these methods that overthrow the traditional paradigm in real data, particularly the extension to unrecognized blends that are not at the same redshift, their mathematical justification is unquestionable. A first application of the method from Bernstein et al. (2016) to the HSC survey will be presented in Armstrong et al. *in prep.*

It is becoming increasingly common for weak lensing surveys to use two shear estimation methods with different assumptions (e.g., DES Y1 results in Zuntz et al. 2017), relying on the comparison to provide some support for the reliability of survey results. A combination

of a "traditional method" calibrated using method (1) or (2), compared with a method in class (4), and an external calibrator like CMB lensing (3), may be necessary to fully justify a belief in the results of Stage-IV lensing surveys at the level of their statistical errors (i.e., without addition of a substantial systematic error budget).

2.8. Photometric redshifts

In this section, I discuss the calculation of photometric redshifts[9], or photo-z's. For weak lensing, what primarily matters is the ability to infer the true redshift distribution for a photo-z-selected sample of galaxies. In other words, there are strong requirements on our knowledge of the photometric redshift errors. I will discuss methods to accurately calibrate the redshift distributions in Section 3.2, while in this section I focus on the photometric redshift estimation itself.

The first step in calculation of photometric redshifts is to measure the input data, which most commonly consists of flux measurements in several photometric bands[10]. For example, consider a galaxy without any color gradients. If the PSF is the same in all bands, aperture photometry might be a perfectly reasonable way to get stable color estimates. Given that the PSF typically differs between the bands, aperture photometry will not give stable color estimates unless the aperture size is large compared to the PSF in the band with the worst seeing, which would result in quite low S/N. As a result, typically some form of PSF-matched aperture photometry (e.g., Hildebrandt et al. 2012) or forced model photometry (with the same model used in each band; e.g., Tanaka et al. 2017) gives better results. More generally, the multi-band photometry must measure light from the same physical area of a galaxy to properly estimate the SED, even if that light comes from a subset of the galaxy (chosen consistently across the bands).

Ideally, these measurements should be made in a way that reduces sensitivity to systematics such as Galactic extinction, seeing, and other observational or astrophysical effects with coherent patterns on the sky. There are some low-level systematics to consider in calculation of the photometry, e.g., variation of the bandpasses across the field-of-view and photometric calibration across the survey including color effects (Li et al. 2016; Burke et al. 2017). For these and other spatially-varying issues such as Galactic extinction, it is not generally the RMS error that is relevant, but rather the spatial correlation function of the errors, which will determine the scales on which the measured two-point correlations will show signatures of these systematics. See Ilbert et al. (2009) for a discussion of technical considerations such as uncertainty in photometry/filter curves.

There are several classes of photometric redshift methods; see Hildebrandt et al. (2010) for a summary of many methods, and Tanaka et al. (2017) and Sánchez et al. (2014) for the methods used for HSC and DES Science Verification, respectively. The two main classes of methods are (1) template-fitting methods, which rely on a set of templates for galaxy SEDs that are used to predict the galaxy photometry as a function of redshift, and can be

---

[9]Many methods produce a photometric redshift posterior probability $p(z)$ rather than a single point estimate. I will nonetheless refer to these indiscriminately as photometric redshifts or photo-z's.

[10]Several papers have suggested using additional morphological information, such as sizes and shapes (e.g., most recently, Soo et al. 2017). Given that these correlate with lensing shear, it is unclear what the impact of this would be for cosmology analyses. For example, if the photo-z errors become systematically correlated with the lensing shear, this could be problematic to correct.

compared with the observed photometry (for a summary, see Ilbert et al. 2006); and (2) machine learning methods, which empirically learn the relationship between photometry and redshift based on a training sample. The key issues for template-fitting methods are insufficiency of the templates to accurately describe the full span of the real data, while the key issues for machine learning methods are the difficulty in generalizing to samples that do not look like the training data. Both of these limitations would be eliminated if we had a very large, perfectly representative spectroscopic training sample – which highlights the fact that the primary limitation for modern photometric redshift methods is the insufficiency and/or non-representativeness of spectroscopic redshift samples to the depth of the lensing surveys (Newman et al. 2015).

There are multiple problems with existing spectroscopic samples. Some regions of color and magnitude space are not well-covered by spectroscopic redshift samples, particularly at the faint end. In principle, reweighting schemes (Lima et al. 2008; Cunha et al. 2009) could mitigate this limitation when training and/or calibrating photometric redshifts, as long as all regions of color and magnitude space have some objects. Unfortunately, this solution may not work because it is not obvious that spectroscopic redshift successes and failures at fixed color and magnitude have the same redshift distribution. This problem is much harder to detect without e.g. obtaining spectra from a different spectrograph that has a different range of wavelengths and sensitivity. Also, since the galaxy samples used for weak lensing have additional selection criteria imposed besides cuts on color and magnitude, it may be necessary to consider this higher dimensional space when training and calibrating photometric redshifts for lensing (e.g., Hoyle et al. 2017; Medezinski et al. 2017). Trying to match this higher dimensional space is challenging given the limited size of current deep spectroscopic samples. Finally, it is possible that some selection criteria used for targeting galaxies for spectra can induce additional non-negligible biases in the redshift distribution, which is problematic when using those redshifts for spectroscopic training and calibration (e.g., Gruen & Brimioulle 2017).

One outstanding problem in the field is photometric redshift training in the presence of unrecognized blends (see Section 2.3). This is a non-trivial problem that requires additional attention from the field as we move towards deeper surveys. One approach may be to ignore this issue in training, and fold it into the catastrophic failure rate when calibrating the photo-z; this places greater demands on the calibration strategy. In addition, the existence of shear selection biases induced by photo-z complicates the analysis of tomographic shear correlations; see Troxel et al. (2017) for a recent example with mitigation schemes.

2.9. Masks and survey geometry

Describing the survey coverage requires a way to describe the exact location of its boundaries – not just edges but also internal boundaries due to e.g. masking bright stars – and the spatial dependence of quantities that determine systematic errors and/or galaxy number densities, such as the depth, PSF size, etc. Several software frameworks have been developed to describe survey geometry, typically with some flexible hierarchical description of geometry. These include Healpix[11] (Górski et al. 2002), Mangle (Swanson et al. 2012), and STOMP (Scranton, Krughoff & Connolly 2007).

There are several places where these descriptions are needed. First, maps of the spatial

---

[11]https://github.com/healpy/healpy

dependence of systematics can be correlated against quantities of scientific interest (e.g., photo-z's or shear estimates) to identify which systematics are most relevant and need further improvement. An example of map-level systematics investigation in the HSC survey was carried out by Oguri et al. (2017). Second, coverage maps can be useful to generate mock observations that have the same coverage as the real data. Since survey boundaries can lead to selection biases and to leakage between E and B-mode power, mock catalogs with the same boundaries can be valuable for systematics investigations. Finally, the optimal estimator for galaxy-galaxy correlations (Landy & Szalay 1993) and galaxy-shear correlations (Singh et al. 2017) requires random points with the same spatial coverage as the real galaxies (but with correlation function equal to zero). This need arises because the optimal estimator involves correlation of the overdensity rather than the density itself, so in each case where the galaxy field is used, a random field is needed also. Moreover, for galaxy-shear correlations, the subtraction of shear around random points not only produces a more optimal estimator, but is useful for subtraction of systematics (Mandelbaum et al. 2005) if the number density-dependence on systematics-generating quantities is faithfully reproduced in the random sample (Mandelbaum et al. 2013). Morrison & Hildebrandt (2015) have demonstrated the impact of systematic variation of galaxy number densities with observational parameters such as depth, extinction, and so on, and the need to model these dependencies beyond linear order to accurately estimate angular correlations from large imaging surveys. This is relevant both for galaxy-galaxy and galaxy-shear correlations that go into a cosmological weak lensing analysis.

The above statements about the need to faithfully reproduce survey boundaries and the dependence of galaxy density on observational conditions is related to arguments made in the literature about the so-called "boost factor" that accounts for the contamination due to (unlensed) physically-associated galaxies used as sources in galaxy-galaxy or cluster-galaxy lensing measurements. This idea was introduced by Sheldon et al. 2004. The difficulty in using this formalism for small-area surveys in practice was presented by Medezinski et al. (2017) and Melchior et al. (2017), with an alternative formalism involving explicit modeling of the smooth redshift distribution and the contribution from physically-associated galaxies given by Gruen et al. (2014). An additional complication is the need to trace the possible difficulties detecting source galaxies in high-density regions (e.g., in galaxy clusters, due to the obscuration of background galaxies by foregrounds; Simet & Mandelbaum 2015).

3. FROM CATALOGS TO SCIENCE

This section covers the steps in a weak lensing analysis from catalogs to cosmological parameters. It is in this phase of the analysis that we must include steps for mitigation of astrophysical uncertainties and any residual observational systematics.

3.1. Estimators

Here I assume the availability of a set of galaxy positions on the sky, per-object shear estimates defined as in Sec. 1, and photometric redshifts. The estimator for the reduced shear will be denoted $\hat{g}$. Typically the coordinate system for $\hat{g}$ is defined such that positive $\hat{g}_1$ corresponds to an East-West or North-South elongation, while $\hat{g}_2$ is defined at $45°$ with respect to that axis. The focus of this section is how to combine these quantities and measure statistics that are cleanly related to the matter distribution.

For shear-shear correlations, galaxies are divided into tomographic bins based on the photometric redshifts. Pairs of galaxies are identified, and their separation on the sky is calculated, including the angle with respect to the sky coordinate axes: separation on the sky $|\theta|$ and polar angle ϕ. For each pair, the relevant shear components are tangential $\hat{g}_+$ and cross $\hat{g}_\times$, with the convention that tangential shear around overdensities results in $\langle \hat{g}_+ \rangle > 0$ and radial shear around underdensities gives $\langle \hat{g}_+ \rangle < 0$. For one of the galaxies with shape $\hat{g}$, we obtain

$$\hat{g}_+ = -\mathrm{Real}[\hat{g} \exp{(-2\mathrm{i}\phi)}] \tag{7}$$

$$\hat{g}_\times = -\mathrm{Imag}[\hat{g} \exp{(-2\mathrm{i}\phi)}]. \tag{8}$$

The estimator for the shear correlation functions $\xi_\pm$ in that tomographic bin is (Schneider et al. 2002)

$$\hat{\xi}_\pm(\theta) = \langle \hat{g}_+ \hat{g}_+ \rangle(\theta) \pm \langle \hat{g}_\times \hat{g}_\times \rangle(\theta) \tag{9}$$

with $\langle \hat{g}_+ \hat{g}_\times \rangle = 0$ due to parity symmetry, and the averages being weighted averages (typically inverse variance weighting, including the intrinsic shape noise and measurement error). This realistic estimator is insensitive to survey masks and boundaries. The theoretical prediction for $\xi_\pm(\theta)$ can be derived as Hankel transforms of the convergence power spectrum,

$$\xi_\pm(\theta) = \int \frac{\ell \, \mathrm{d}\ell}{2\pi} J_{0/4}(\ell\theta)[P_\kappa^{(\mathrm{E})}(\ell) \pm P_\kappa^{(\mathrm{B})}(\ell)]. \tag{10}$$

To lowest order, lensing produces only E-mode power (a pure gradient field), but there are low-level physical effects that cause B modes (corresponding to a curl component; see Section 3.3). Certain systematics can manifest as mixes of E and B modes, and detection of B-mode power is one way to identify those systematics; however, not all systematics produce B modes.

Since lensing produces primarily E-mode power, and the power estimated in each ℓ bin should be roughly independent, there is interest in directly estimating the power spectrum. However, the most naive way of doing so involves measuring shear correlations over all scales, and in practice, the lack of pairs on small scales and the finite sizes of lensing surveys leads to a mixing of E and B modes (Kilbinger, Schneider & Eifler 2006). There are so-called pseudo-power spectrum estimators (e.g., Hikage et al. 2011) that aim to mitigate this effect and enable direct estimation of the power spectrum. There are additional configuration-space estimators, and estimators that combine the estimated $\hat{\xi}_\pm(\theta)$ with various filters in ways that are meant to be more optimal (e.g., Asgari, Schneider & Simon 2012). No matter what estimator is used, models for systematic uncertainties must be re-expressed in terms of those estimators in order to marginalize over and remove the uncertainties.

The above discussion was focused on shear-shear correlation functions. However, as mentioned previously, the canonical weak lensing analysis for future surveys will include galaxy-shear and galaxy-galaxy correlations, defined within tomographic bins in analogous ways. When constructing these estimators using the galaxy overdensity field, they have contributions from both clustering and magnification. Bernstein (2009) presents the relationship between empirical estimators of these three two-point correlation functions and the underlying theoretical quantities: lensing shear, magnification, and galaxy overdensity.

When choosing estimators for the galaxy-shear and galaxy-galaxy correlations, there are different philosophical approaches. On small scales, these correlations depend on how galaxies populate dark matter halos. One family of estimators removes the small-scale

information to avoid systematic uncertainty in cosmological constraints due to astrophysical details (e.g., Baldauf et al. 2010). Other approaches are to include the small scales, build models with nuisance astrophysical parameters, and marginalize over them (e.g., Yoo et al. 2006; van den Bosch et al. 2013). The choice of which type of estimator to use depends on the users optimism in their ability to describe these astrophysical uncertainties with sufficient realism to avoid substantial systematic errors while using a simple model.

Data compression from shear correlations or power spectra may be possible and even desirable. The number of data points in the estimator places serious demands on covariance matrix estimation (Section 3.6) and the cosmological parameter inference method (Section 3.7). For that reason, investigation of data compression methods such as those recently proposed for galaxy power spectra may be beneficial (Gualdi et al. 2017).

Finally, for the case of shear-shear correlations, a 3D lensing approach that avoids the need for tomographic binning has been proposed and used in real data (Simon, Taylor & Hartlap 2009; Kitching, Heavens & Miller 2011; Kitching et al. 2014). However, future work is needed on how to use this in a joint analysis with galaxy-shear and galaxy-galaxy correlations, and properly marginalize over systematics.

3.2. Redshift distributions and bins

Section 2.8 described photometric redshifts, defined either as point estimates or posterior probability distributions $p(z)$. This section will explain how they are used for science. A variety of schemes exist for dividing galaxies into tomographic bins, e.g., based on division of the sample using the point photo-z estimates. Determination of the true ensemble redshift distribution[12], or $N(z)$, is critical for cosmological analyses. To lowest order, weak lensing is primarily sensitive to the mean redshift and the width of the redshift distribution of each tomographic bin (Amara & Réfrégier 2007); this fact is often used to motivate how nuisance parameters for redshift uncertainty are included in the cosmological analysis (e.g., DES Collaboration et al. 2017). The inclusion of catastrophic photometric redshift errors complicates this issue (Hearin et al. 2010).

In general, spectroscopic redshifts are needed for photo-z training (Sec. 2.8) and calibration, where the type of redshift samples needed for these purposes differs (Newman et al. 2015). The typical required redshift sample size is of order 10^5 in order to reduce the systematic uncertainty on mean redshifts in tomographic bins to the $\sim 10^{-3}$ level that is needed to avoid Stage IV surveys being systematically biased at a level exceeding the statistical uncertainties. There are two methods for using spectroscopic redshifts to calibrate the $N(z)$ of photometric redshift samples. The first is to reweight the spectroscopic redshifts to match the observed properties of the photometric sample (Lima et al. 2008) and directly infer the $N(z)$, though there is some debate as to which sample properties should be used for that reweighting (see, e.g., Medezinski et al. 2017). Previous studies have explored the spectroscopic redshift sample size needed for direct calibration of $N(z)$, without (Ma & Bernstein 2008) and with catastrophic errors (Sun et al. 2009; Bernstein & Huterer 2010). Generically, this method requires a spectroscopic redshift sample that covers all of the photometric color and magnitude space (not necessarily evenly, with reweighting accounting for

---

[12]While it is tempting to stack the per-object $p(z)$, which is a mathematically acceptable approach to using spectroscopic redshifts, stacking per-object $p(z)$ violates the definitions of probability (Malz et al. *in prep.*). It is nonetheless often done.

the non-representativeness of the spectroscopic redshift sample). An additional assumption is that the $N(z)$ at fixed color and magnitude is the same for spectroscopic successes and failures, which is likely incorrect at some level. The resulting systematic uncertainty is difficult to estimate and is often ignored for current datasets. Beck et al. (2017) proposes a framework for exploring this assumption for shallow surveys. The extension of this test to deeper surveys (where degeneracies between high and low redshift may be more important in determining spectroscopic success) is of critical importance for future surveys that wish to rely on spectroscopic reweighting to determine the $N(z)$ of photometric redshift samples.

The second method is to use the cross-correlation between the photometric redshift sample and some non-representative spectroscopic redshift sample covering the full redshift range of the photometric sample with large enough area and sampling rate to allow the clustering cross-correlation to be well-determined. Several variations on the cross-correlation or clustering redshift method have been proposed (Newman 2008; Benjamin et al. 2010; McQuinn & White 2013; Ménard et al. 2013; Schmidt et al. 2013). Differences between them include the choice of scales to use (purely linear bias scales, or small scales as well); the method of modeling the galaxy bias for the photometric sample; and the corrections for magnification bias, which induces nonzero correlations between galaxies in bins that truly are separated in redshift. Recent results using this approach include Choi et al. (2016); Morrison et al. (2017); Johnson et al. (2017).

Because of the different assumptions behind these two methods, DES and KiDS used both to calibrate their $N(z)$ (Hoyle et al. 2017; Hildebrandt et al. 2017), though for DES they used subsets of luminous red galaxies with high-quality photo-z's rather than spectroscopic redshifts when carrying out the cross-correlation analysis, and also used high-quality 30-band COSMOS photo-z's for the direct $N(z)$ calibration. It seems likely that in future, both methods will continue to be used so as to have a cross-check on the resulting calibrated $N(z)$.

The needs for additional spectroscopic redshift samples for photo-z training and calibration for future surveys is summarized in Newman et al. (2015). Techniques have been proposed for how to identify the regions of color/magnitude space that should be targeted to fill in missing regions of parameter space (including self-organizing maps, Masters et al. 2015, which were used for targeting a new spectroscopic survey in Masters et al. 2017).

Finally, the difficulty in calibrating $N(z)$ is connected to the exact analysis being done. Use of galaxy-shear, galaxy-galaxy, and shear-shear correlations together may result in less stringent needs for spectroscopic redshift calibration samples, while the need to jointly model intrinsic alignments may result in more stringent requirements for how well we understand photometric redshift uncertainties (Joachimi & Schneider 2009). An additional issue of relevance especially for deep ground-based surveys is the role of blending systematics (Section 2.3), which have the potential to increase the catastrophic photometric redshift error rate. Since small-area spectroscopic redshift samples may have targeting criteria that avoid obvious blends, the impact of blending on photometric redshift errors may need to be assessed primarily through the cross-correlation method.

3.3. Theoretical predictions

To constrain cosmology with weak lensing measurements, theoretical predictions with an accuracy of ~1% over a wide range of scales and cosmological parameters are needed (e.g., Huterer & Takada 2005). To interpret the shear-shear correlations alone, predictions for

the distribution of dark matter are needed, while joint interpretation with galaxy-shear and galaxy-galaxy correlations requires a way of describing the distribution of galaxies.

Weak lensing measurements typically go quite far into the nonlinear regime, so an accurate description of the nonlinear matter power spectrum is required. This description can come from large suites of N-body simulations with many values of cosmological parameters, and some manner of interpolating between the values of parameters for which simulations were generated. One option is to use simulations to calibrate a fitting formula (e.g., halofit: Takahashi et al. 2012). Another approach is to use an emulator, such as Heitmann et al. (2014), which interpolates over cosmological parameter space using Gaussian processes. While fitting formulae and emulators have tremendous value in enabling fast, accurate calculations of the matter power spectrum, using simulations directly can help (a) enable inclusion of physical effects that might be difficult to incorporate through an analytic approach and which depend on cosmology, such as density-dependent selection effects (e.g., Hartlap et al. 2011); (b) allow for joint modeling with galaxy correlations; and (c) include higher-order theoretical nuances.

When modeling the galaxy-shear and galaxy-galaxy correlations, the simplest assumption to make is that the galaxy bias is linear (galaxy and matter overdensities are related as $\delta_g = b\,\delta$) and that the galaxy and matter overdensities are perfectly correlated, $r_{\rm cc} = P_{\rm gm}/\sqrt{P_{\rm gg}P_{\rm mm}} = 1$. These simple assumptions are valid at large separations, and fail for a variety of reasons on small scales. They were used in the joint analyses of the three galaxy and shear auto- and cross-correlations from DES and KiDS (DES Collaboration et al. 2017; van Uitert et al. 2017). In DES, to avoid sensitivity to systematics from the linear bias assumption, the choice was made to limit the analysis to relatively large scales, > 8 and $> 12h^{-1}$Mpc for galaxy-galaxy and galaxy-shear correlations, respectively. In both cases, tests were carried out to assess the sensitivity of the results to this assumption.

For future surveys, the measurements will have sufficient signal-to-noise that it will be necessary to adopt more realistic models. One option is a perturbation theory-based model for $b(k)$ and $r_{\rm cc}(k)$ (e.g., Baldauf et al. 2010), which has been used for a galaxy-shear and galaxy-galaxy joint analysis in SDSS (Mandelbaum et al. 2013). Another option is a halo model approach, which provides a numerical description for the galaxy-matter and galaxy-galaxy correlations based on how galaxies populate dark matter halos (e.g., Yoo et al. 2006; van den Bosch et al. 2013), and which has been used in practice for interpretation of BOSS galaxy lensing and clustering (More et al. 2015). As mentioned in Section 3.1, the choice of the estimator to use for the measurement is related to the question of how the modeling is to be done, because some model descriptions can go to smaller scales than others. In addition, it may be necessary to consider how higher-order complexities like assembly bias (wherein the galaxy bias depends on more than just the mass) complicates the joint analysis of galaxy and shear correlations, specifically assumptions about $r_{\rm cc}$ and its scale dependence. Preliminary steps towards understanding this issue have already been made (e.g., McEwen & Weinberg 2016). For future surveys, calibration of how $b(k)$ and $r_{\rm cc}(k)$ are modeled against realistic mock galaxy catalogs will be crucial for choosing what range of scales can be used and ensuring accurate cosmological constraints.

For the prediction of projected lensing statistics, there are a number of low-level theoretical issues that have not been relevant for past and ongoing lensing surveys, but which may require attention in upcoming surveys. These include the distinction between shear and reduced shear, the impact of several approximations (flat sky, Born, Limber, linearized gravity, and Hankel transform) and higher order lensing terms, lens-lens coupling, and
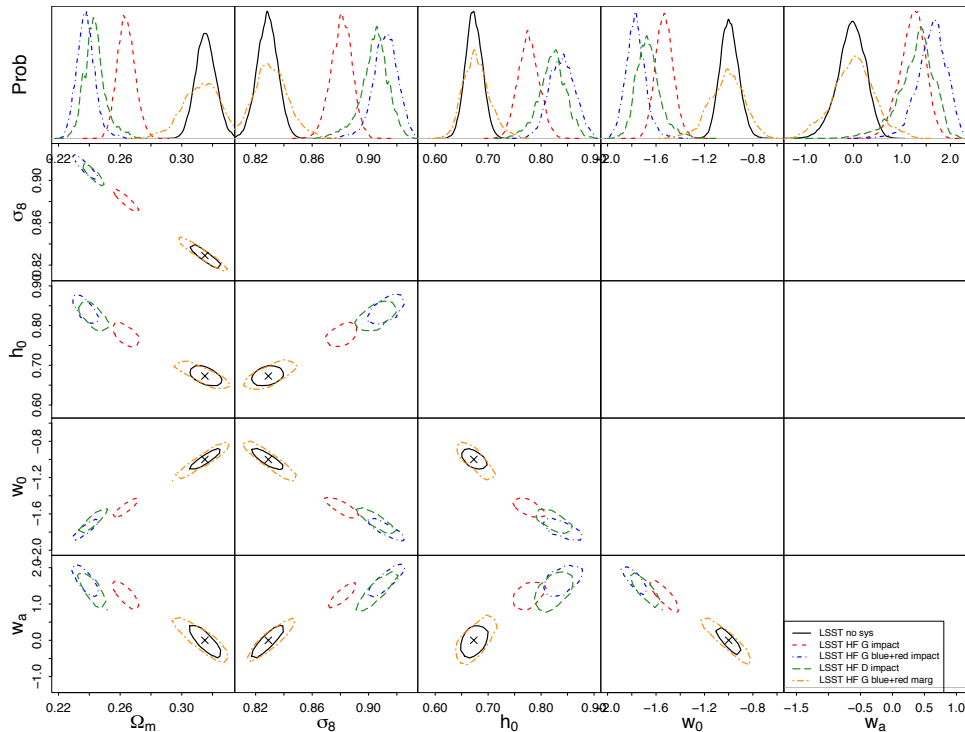
Figure 7: An illustration of the impact of intrinsic alignments on cosmological parameter constraints with weak lensing in LSST, using shear-shear correlations only (from Krause, Eifler & Blazek 2016). The bottom left triangle shows the 2D contours for cosmological parameters, where the black curve shows the case of no intrinsic alignments; red, green, and blue curves show intrinsic alignments predictions with different ways of modeling the alignments of blue and red galaxy populations and their luminosity evolution; and the orange curve shows how the constraints become less tight when marginalizing over the intrinsic alignments. The top row shows the posterior probabilities for each of the cosmological parameters. Clearly the biases without marginalization are unacceptably large.

source clustering-induced B modes (Bernardeau 1998; Schneider, van Waerbeke & Mellier 2002; Dodelson, Shapiro & White 2006; Hilbert et al. 2009; Bernardeau, Bonvin & Vernizzi 2010; Krause & Hirata 2010; Giblin et al. 2017; Kilbinger et al. 2017; Kitching et al. 2017; Lemos, Challinor & Efstathiou 2017; Petri, Haiman & May 2017). Fast methods have been developed for ray-tracing through N-body simulations (Barreira et al. 2016) to avoid some of these approximations, and to incorporate some of the second-order effects (Becker 2013). These effects can enter in different ways to the galaxy-shear correlations, e.g., because of lensing deflections modifying observed positions.

3.4. Intrinsic alignments

Since recent reviews have covered the physics of intrinsic alignments, their impact on weak lensing cosmology, theoretical models, and observations (Joachimi et al. 2015; Kirk et al.

2015; Kiessling et al. 2015; Troxel & Ishak 2015), this section will be brief.

Intrinsic alignments, the coherent alignment of galaxy shapes due to physical effects other than lensing, are a major theoretical uncertainty for weak lensing (Croft & Metzler 2000; Heavens, Refregier & Heymans 2000; Lee & Pen 2000, 2001; Catelan, Kamionkowski & Blandford 2001). Since lensing analyses must assume that coherent shape alignments are due to lensing, intrinsic alignments can contaminate lensing analyses. Theoretical prediction of intrinsic alignments is difficult because, while simulations and analytic models show that dark matter halos have intrinsic alignments in the ΛCDM paradigm, the question of whether observed galaxy shapes (the baryonic components) also show such alignments cannot be answered with N-body simulations. Depending on assumptions made about the galaxy population and the alignments of its baryonic components with the underlying matter field, the predicted level of alignments can vary by orders of magnitude (e.g., Heymans et al. 2006b). However, observations have substantially narrowed this wide variation by placing constraints on the large-scale alignment model for red galaxies, and (so far) null detections of large-scale shape alignments for blue galaxies. Since red galaxies exhibit alignments consistent with their shapes being aligned with the shapes of the inner regions of their halos, high-resolution N-body simulations may indeed be populated with red galaxies that have realistic alignments with the underlying matter density field (e.g., Schneider, Frenk & Cole 2012). Recent work has also included comparison of measured galaxy alignments with high-resolution, large-volume hydrodynamic simulations that include the physics of galaxy formation (Velliscig et al. 2015; Tenneti, Mandelbaum & Di Matteo 2016; Chisari et al. 2017; Hilbert et al. 2017); the simulations broadly reproduce many of the alignment trends seen in real data, but not all of them.

Initial efforts to remove intrinsic alignments from lensing measurements focused on the removal of close galaxy pairs (in 3D: King & Schneider 2002; Heymans & Heavens 2003). However, intrinsic alignments can coherently anti-align galaxies that are well-separated along the line-of-sight. Hirata & Seljak (2004) highlighted the importance of this effect, and subsequent observational work confirmed that it is the dominant impact of intrinsic alignments on weak lensing measurements; but it cannot be eliminated by removing galaxy pairs at the same redshift from the lensing sample. Based on recent observational constraints (e.g., Singh & Mandelbaum 2016), intrinsic alignments will be an important systematic that surveys like LSST must mitigate (Figure 7). Efforts to remove this systematic typically include joint modeling or self-calibration using joint analysis of galaxy-galaxy, galaxy-shear, and shear-shear correlations (Joachimi & Bridle 2010; Yao et al. 2017). These approaches rely on the fact that the various contributing terms have different redshift dependencies, spending some of the statistical constraining power of the data to marginalize over the intrinsic alignments terms.

Current work on intrinsic alignments includes attempts at better observational constraints (requiring redshift estimates and shape measurements), model building (e.g., Blazek, Vlah & Seljak 2015; Blazek et al. 2017), and tests of mitigation methods. Of particular value would be large-area spectroscopic samples that would enable better priors to be placed on the parameters of intrinsic alignment models at redshift $z \gtrsim 0.7$ and at typical galaxy luminosities. While the types of redshift samples that are often proposed as a solution to the problem of calibrating the ensemble redshift distributions may be helpful in principle, it depends on the survey layout (multiple small pencil-beam surveys can be used for redshift calibration, while large-scale intrinsic alignments studies require larger area).

3.5. Baryonic effects

The impact of the physics of galaxy formation on weak lensing observables has been a subject of study for more than a decade. Unfortunately, thorough investigation of this topic requires hydrodynamic simulations that have realistically complicated models of galaxy formation (without the over-cooling problem), high enough resolution to ensure their convergence for typical galaxy masses, and large enough volume to study the impact on the matter power spectrum on cosmological distance scales. This combination of scenarios has only recently become possible, in families of very expensive high-resolution simulations with box lengths of order 100 Mpc, including the EAGLE simulations (Schaye et al. 2015), Illustris (Vogelsberger et al. 2014), and MassiveBlack-II (Khandai et al. 2015).

One approach to account for the impact of baryons on the matter power spectrum is to include them in a perturbation theory-based model for the power spectrum, with baryonic physics producing higher-order terms that can be marginalized over (Mohammed & Seljak 2014). There is also a halo model approach, which has nuisance parameters describing the change in internal structure of dark matter halos, specifically their concentration, due to baryonic physics (Semboloni et al. 2011; Zentner et al. 2013). The extension of a halo model to quite small scales is simpler in practice than the extension of the perturbation theory-based model mentioned above, which requires the inclusion of many additional terms. Zentner et al. (2013) found that for future lensing surveys, additional mitigation may be needed, possibly reflecting the fact that a change in halo concentration is not the only impact of baryonic physics. A halo model approach with changes in halo concentrations and a mass-dependent 'halo bloating' parameter (Mead et al. 2015) has been quite successful in describing the matter power spectrum to small scales; the parameters of that model were calibrated to maximize the fidelity of reproduction of the matter power spectrum, rather than to accurately describe dark matter halo profiles. This approach was adopted by the KiDS survey (Hildebrandt et al. 2017) to model shear-shear correlation functions.

Rather than adopting a physically-motivated approach, Eifler et al. (2015) used an empirical PCA approach. Using a set of cosmological hydrodynamic simulations to construct PCA components that describe the impact of baryonic physics on the dark matter power spectrum, they showed that excluding the first four PCA components is sufficient to mitigate the impact of baryonic physics on a shear-shear correlation function measurement, even going to relatively small scales ($\ell \sim 5000$).

While current results seem to indicate that the impact of baryonic physics on shear-shear correlations is under control for current surveys, and the methods that already exist are promising for future (Stage-IV) surveys, there remain some questions in the field. In particular, for the tomographic shear-shear, shear-galaxy, galaxy-galaxy joint analysis that is likely the fiducial weak lensing analysis for upcoming surveys (due to how it enables marginalization over shear-only systematics), the production of theoretical models that self-consistently include the impact of baryonic physics on all three correlation functions is less well-developed. The halo model and extensions of the PCA approach are promising avenues for investigation. The scales on which these approaches work for the full joint analysis is likely to determine the maximum usable ℓ or minimum usable θ. Additional questions for investigation include the interaction between marginalization over baryonic effects and other systematics. For example, if intrinsic alignment models are constructed separately for red and blue galaxies, such that theoretical models separately predict the signal for the two populations and then take the appropriate weighted averages, then does the baryonic physics model for galaxy-shear and galaxy-galaxy terms also need to differ

for the two populations? This and other interactions (e.g., photometric redshift errors and their uncertainties also depend on the galaxy type) remain to be explored.

3.6. Covariances

The process of inferring cosmological parameters given a set of measurements typically involves knowing the covariance matrix of those measurements, under the assumption that the likelihood function of the observable quantities is a Gaussian. Computing the covariance matrix for weak lensing measurements is a task for which multiple approaches exist in the literature[13], and additional development will be needed for upcoming surveys. In principle, future surveys may have data vectors with of order 1000 points, considering some number of tomographic bins, bins in angular scale or wavenumber, and the three different types of correlations to be measured. Several studies have argued that the number of simulation realizations of upcoming surveys needed to estimate the covariance matrix with sufficient accuracy through brute force methods is prohibitively large (Dodelson & Schneider 2013; Taylor, Joachimi & Kitching 2013), though see recent work by Sellentin & Heavens (2017) that argues those were significantly overestimated in the case that one can parameterize the covariance in some compact way and use the simulations to constrain that parameterization (see discussion below).

The covariance matrix in general has shot noise terms and cosmic variance terms, including contributions from connected four-point functions and supersample covariance (Li, Hu & Takada 2014; Mohammed & Seljak 2014). See Singh et al. (2017) for a recent derivation of the generic covariance expression for two-point correlations of either densities and overdensities, and quantities such as shear. Because some of these terms are cosmology-dependent, in principle, the covariance matrix itself should be re-estimated at each step of a likelihood analysis to constrain cosmology (Eifler, Schneider & Hartlap 2009).

Numerical estimation of the covariance matrix using theoretical expressions is a natural way to incorporate the cosmology-dependence of the covariance. However, ensuring the numerical stability of all terms in the covariance matrix estimation can be quite expensive (e.g., Krause et al. 2017). Hence, building an emulation tool that would enable fast estimation of these covariances would be highly valuable. Most lensing analyses to date have not incorporated a full cosmology-dependent covariance, with the notable exception of Jee et al. (2013) for non-tomographic shear-shear correlations only. In the KiDS analysis that included shear-shear, shear-galaxy, and galaxy-galaxy correlations (van Uitert et al. 2017), the cosmology-dependence of the covariance was partially accounted for through an iterative procedure. While they did not vary the covariance at each step of their MCMC, they did use the best-fitting cosmology from their first MCMC to regenerate the covariance and then rerun the fitting procedure.

Another approach that has seen popularity with past surveys is direct empirical estimation of the covariances, such as using the jackknife or bootstrap method, with the subsamples consisting of large contiguous regions within the survey (e.g., Mandelbaum et al. 2013). This approach has been rigorously compared with both numerical estimates of covariances and with realistically complex mock catalogs for galaxy-shear and galaxy-galaxy correlations (Shirasaki et al. 2017; Singh et al. 2017), and has been found to be quite accurate for

---

[13]Some of these approaches were developed for shear-shear correlations, and the extension to galaxy-shear and galaxy-galaxy requires additional work.

scales up to the size of the jackknife regions. A natural tension for this method is that the need for the number of regions to significantly exceed the number of data points motivates the use of many smaller regions, but use of smaller regions reduces the range of scales on which the jackknife can be accurately used, and causes a violation of the assumption of region independence. However, if a given survey configuration allows the jackknife method to be used, it can be useful in avoiding the need for many realizations of mock catalogs. The covariance matrix estimated in this way will be noisy, and since the inverse covariance used for likelihood analysis is then biased, the sizes of cosmological parameter constraints must be corrected (e.g., Hirata et al. 2004; Hartlap, Simon & Schneider 2007) .

In principle, using many simulation realizations of the survey provides a way to estimate covariance matrices. Similarly to the above empirical methods, each element of the covariance matrix must be independently constrained, and hence longer data vectors pose a greater challenge. For expected data vectors in the surveys of the 2020s, the number of realizations needed to do this as a function of cosmology is likely prohibitive, even assuming the expected increase in computing power available in the 2020s. The noise resulting from the limited number of realizations compared to the number of data points (Blot et al. 2016) must also be taken into account, e.g., using the methods mentioned above for empirical covariances. However, it is more likely that a hybrid approach will be used, adopting some method for modeling the covariance and then constraining its (much smaller number of) parameters using the simulations. For example, methods for modeling the precision matrix (inverse covariance matrix; Padmanabhan et al. 2016; Friedrich & Eifler 2017) or perturbation theory approaches to the covariance (Mohammed, Seljak & Vlah 2017) may be useful, in addition to simulation-calibrated versions of the numerical models mentioned above. Techniques for fast mode resampling may also be useful in reducing the number of simulation realizations needed (Schneider et al. 2011). Finally, data compression methods introduced in Sec. 3.1 are also relevant here. In the coming years, it will be important that a way forward that works for the full tomographic shear-shear, galaxy-shear, and galaxy-galaxy analysis be validated and implemented; see Marian, Smith & Angulo (2015) for a demonstration of some issues that arise when combining galaxy-shear and galaxy-galaxy correlations and estimating covariances. Ideally, a fast emulator (e.g., building on ideas from Morrison & Schneider 2013) would be constructed, to avoid cosmology-dependent covariance matrix estimation being a primary limiting step in the final likelihood analysis.

3.7. Inference

Cosmological inference from weak lensing with past and current datasets has typically involved the assumption that the likelihood function of the observables in Gaussian, and use of some form of Markov Chain Monte Carlo (Lewis & Bridle 2002; Feroz, Hobson & Bridges 2009; Foreman-Mackey et al. 2013) to sample parameter space and identify best-fitting parameters and confidence intervals. It may also be important for future surveys to account for non-Gaussianity in the likelihood (e.g., Sato et al. 2009, 2011).

One of the key challenges facing future surveys in the cosmological parameter inference step is the high dimensionality of the problem. The multiple tomographic bins and three correlations to jointly model produce of order 1000 data points. The number of systematics that must be marginalized over will be of order 100, in addition to of order 10 cosmological parameters. While alternative inference methods have been proposed (e.g., Jasche & Wandelt 2013; Lin & Kilbinger 2015; Alsing et al. 2016), substantially more research must be

done to ascertain the feasibility of adopting them for future cosmological lensing surveys. Some of these methods come with the substantial benefit that one can avoid the Gaussian likelihood assumption and covariance matrix estimation, typically at the cost of requiring fairly realistic forward simulation techniques for the observable quantities.

One issue that has received significant attention in the weak lensing community is confirmation bias (e.g., Croft & Dailey 2011), the solution for which is to carry out a blinded analysis until null tests are passed and decisions have been made about what range of scales and models to use. All three ongoing weak lensing surveys have adopted a blind cosmological analysis strategy (DES Collaboration et al. 2017; Hildebrandt et al. 2017; Mandelbaum et al. 2017b). The details depend on the survey and the analysis being carried out, and most surveys adopt a combination of the following: (a) applying a randomly selected calibration factor to the shears, (b) having multiple catalogs with randomly selected calibrations and only one person able to reveal which of those catalogs is the true one (zero additional calibration factor), (c) applying random calibration factors to the measured two-point correlations, (d) avoiding plotting the data against predictions from any cosmological model, (e) looking at MCMC results only after subtracting off the best-fitting cosmological parameters, i.e., $\Delta\Omega_m$ rather than Ω_m itself. Some of these strategies may only work with current datasets (where cosmological parameter changes look close enough like calibration offsets), but not future data (where changes in shape of the two-point correlations with cosmology will be evident due to the smaller errors). The common adoption of blind analysis methods is a positive step forward for the field of weak lensing, and current surveys should be quite informative as to which methods are likely to work for future surveys.

4. DETECTING AND MODELING OBSERVATIONAL SYSTEMATICS

In this section, I discuss the classes of systematic errors, and the tests that can help reveal them using the data itself. For survey papers that use many systematics tests to reveal observational systematics, including 'null tests' (which should be zero in the absence of systematics), see Hildebrandt et al. (2017); Mandelbaum et al. (2017b); Zuntz et al. (2017). Here I will not discuss null tests for PSF modeling errors, which were thoroughly discussed in Sec. 2.1 of this review. Before considering specific null tests, it is worth noting a general rule that null tests are often most informative when carried out after binning samples based on any independent quantity that could be related to a potential systematic.

As mentioned in Sec. 3.3, cosmological B modes are expected to be quite small, and hence a detection of non-zero B-mode power is typically interpreted as arising from systematics. Unfortunately, B modes can have many origins, including PSF modeling errors, PSF correction errors, astrometric errors, and intrinsic alignments. Uncovering which of these is responsible can be difficult, and the correct mitigation scheme to use depends on the origin of the effect (Hildebrandt et al. 2017). Also, many systematics do not generate B modes, and hence a lack of B modes does not guarantee a systematics-free measurement.

Another common diagnostic for additive biases, the star-galaxy correlation function, can be nonzero for a number of reasons. This test involves correlating the shapes of stars with the PSF-corrected galaxy shear estimates. Thus, both PSF modeling errors and insufficient PSF correction of galaxy shapes can contribute. This test has been used in different ways in previous lensing measurements. The zero-lag star-galaxy correlation can be estimated using the PSF model shape for the "star" shape, and averaged within small regions (Heymans et al. 2012; Hildebrandt et al. 2017). Assigning an uncertainty on this quantity generally

requires using mock catalogs that have a realistic level of cosmic variance and PSF model variation across the fields. This test was used in CFHTLenS to eliminate outlier fields that (for undetermined reasons) were too systematics-dominated to use for science. An alternative approach (Mandelbaum et al. 2017b) is to measure the full star-galaxy shape correlation as a function of separation, averaged over the entire survey. In principle, this should be the sum of terms from PSF modeling errors (related to the ρ statistics) and from uncorrected PSF anisotropy. It provides a template for marginalization over additive errors due to these systematics; however, leakage across the star-galaxy boundary can result in this correlation including cosmic shear as well.

Correlations with systematics maps is another method that can enable the detection of observational systematics (Chang et al. 2017; Oguri et al. 2017). This method involves producing lensing mass maps from the shear catalog, and maps corresponding to the values of any quantity that may be considered as a possible cause for weak lensing systematics (e.g., stellar density, PSF FWHM, PSF shape). The cross-correlation between the lensing and systematics maps should be zero in the absence of systematics. Map-level correlations can be a more compact way to detect certain systematics, rather than re-computing all 2-point correlation null tests after dividing the sample into bins in seeing and other quantities (as was done in, e.g., Becker et al. 2016).

Calculating average shears with respect to arbitrary locations that should not generate lensing shear is another common null test. For example, the average shapes of galaxies with respect to the CCD coordinate system or the positions of stars should be zero (modulo noise and the contamination of the star sample with galaxies). The caveat in the parenthesis highlights another important point, which is that the origins of deviations from zero for null tests should be carefully considered. Sometimes the source of the signal observed is completely different from what was originally intended.

There are few null tests that are meant to specifically identify residual detector effects. A recent example is the computation of PSF model size residuals as a function of stellar magnitude (Mandelbaum et al. 2017b; Zuntz et al. 2017). Computing the mean shear in CCD coordinates for galaxies binned based on their CCD row/column can also be useful for identifying detector systematics (e.g., Huff et al. 2014; Zuntz et al. 2017). The development of more tests that can identify failure to correct for detector effects or chromatic PSF effects would be useful for the next generation of surveys, which require a greater level of control over those effects.

One useful tool to detect systematics due to nearby galaxies and/or due to failures in the analysis pipeline is to inject fake galaxies into real data and rerun the analysis pipeline (Suchyta et al. 2016; Huang et al. 2017). Comparison of the measured properties of the fake galaxies with the input ones can help diagnose problems with many steps of the analysis pipeline (detection, deblending, photometry, shear estimation). The impact of the injected galaxies on the real ones can also be measured; while we do not know ground truth for the real galaxies, the difference between the originally-measured properties and those measured after injection of the fake objects can be revealing (Samuroff et al. 2017).

Unfortunately, there is no observational test to identify failures in the absolute multiplicative calibration of the ensemble shear signal, which is why the problem described in Section 2.7 has attracted so much attention. However, comparing subsamples of galaxies can reveal relative calibration biases between subsamples, modulo selection bias (Section 2.5), which makes the division into subsamples a potentially problematic null test. In other words, for this to be a useful test, the standard sources of bias such as noise bias, model

bias, and selection bias must be separately calibrated out for the subsamples in order to use this as a test for unrecognized/unknown systematics. One important aspect of shear comparisons (whether between subsamples within a given survey, or between the same sample of galaxies measured in two surveys) is that they should always happen at the level of ensemble shears, not per-galaxy shapes, for the reasons explained in Section 2.7. See Amon et al. (2017) for one example of a recent shear comparison, with methodology that should be applicable elsewhere. This comparison can be done at the level of ensemble shear estimates for matched samples with a common set of photo-z's, to identify shear-related calibration offsets, or at a higher level that includes both photo-z and shear-related calibration offsets.

To identify and remove additive systematics due to physical effects associated with specific exposures or surveys (e.g., atmospheric PSFs, or a detector effect), one possible way forward is to cross-correlate shear maps from different surveys or subsets of exposures within a single survey. In principle, this test could be extended not just to consistency tests (i.e., split the LSST exposures into two sets, and do a separate analysis in each one), but to detect and exclude data with potentially unknown systematic errors (i.e., through a jackknife process that involves sequentially excluding small portions of data and testing their statistical consistency with the rest).

The above tests (and the ρ statistics described earlier in this review) and analysis of survey simulations can be used to identify the presence of systematics that can contaminate cosmological weak lensing analysis. They will also provide templates for residual systematics that can be marginalized over when constraining cosmological parameters. It is important that these template not only be scale-dependent, but also galaxy property-dependent and/or redshift-dependent, since most shear systematics will depend on the galaxy properties at some level, and hence on the redshift. Indeed template marginalization is a popular method for removing theoretical systematics, but unlike for observational systematics, there are fewer null tests that can be done for theoretical systematics (with typical tests being eliminating data in regions where the systematics should be worse, and testing for consistency of results).

5. SUMMARY

The high-level goal of this review is to answer the following question: "What does the weak lensing community need to do in order to get to the point where surprising claims that are made about dark energy with LSST, Euclid, or WFIRST will be believed?"

The fact that LSST, Euclid, and WFIRST are designed in ways that result in different dominant systematics is an important aspect of the landscape of the 2020s. For example, Euclid's broad RIZ filter means that it is far more susceptible to chromatic effects (Section 2.1) than LSST or WFIRST. The WFIRST survey design is more conservative than Euclid in terms of the number of samples at each position, making it less likely to suffer from undersampling (due to, e.g., cosmic rays that result in an exposure being excluded). WFIRST's NIR detectors will have different pixel-level systematics than the Euclid or LSST CCDs, and greater calibration challenges due to the CMOS architecture. LSST will suffer from blending far more than the two space-based surveys. The fact that Euclid is shallower than WFIRST or LSST means that it can more easily gather representative spectroscopic samples for photometric redshift training and calibration. However, the fact that WFIRST will be completely within the LSST footprint (and will use it for photometric redshift determination) results in greater survey homogeneity than Euclid, which will rely

on several ground-based datasets for photometric redshifts. Relying on the various survey cross-comparisons plus the fact that they suffer from systematics at different levels will be highly scientifically valuable, and the combination of the surveys has the potential to be even more powerful than one would expect by naively combining statistical errors (Jain et al. 2015, Rhodes et al. *in prep.*).

Below are a number of key take-aways synthesizing the material in the sections above:

1. There are low-level issues such as detector systematics, chromatic effects, astrometry, and survey geometry representation for which work is clearly needed to get where we need to be for surveys in the 2020s, but there are promising avenues for investigation.

2. An area where genuinely new ideas are needed is blending systematics, both in how to quantify and mitigate the impact of low-level blends on shear and photo-z, and the impact of unrecognized blends. The field has only recently started to confront this issue, and more work is needed.

3. Several issues fall into the category of "promising ideas exist but more exploration is needed to determine which will work and how exactly to use them at the level of precision needed for future surveys": calibration of $N(z)$ for photometric redshift samples, shear calibration, optimal image combination, PSF modeling, mitigation of theory systematics, and covariance matrix estimation. Serious work must be done by the community, but all of these issues are more advanced than blending systematics. The calibration of $N(z)$ for photometric redshift samples has gotten less attention than shear calibration until recently, and therefore there is some catching up to do in this area. Indeed, the weak lensing community's unfortunate habit of outsourcing photo-z production and calibration without considering the cross-talk between shear-related selection effects and photo-z's must end: we must interface with the photo-z community at an earlier phase of the analysis.

4. Decisions to be made about image combination must factor in the connection between image combination, PSF modeling, shear estimation, and deblending.

5. Choice of data compression methods will have an impact on the best way to handle covariance matrix estimation and cosmological parameter inference.

6. The field views shear estimation quite differently from how it did from the mid-1990s until around 2012: it is now well-understood that estimation of per-galaxy shapes will not result in an unbiased estimate of the ensemble shear, so the focus is on either calibration strategies or methods of inferring shear without per-galaxy shapes. Several highly promising options currently exist.

7. Regarding the overall cosmological inference problem, more work is needed on blinding strategies for weak lensing analysis by upcoming surveys. In addition, there is still room to draw the field away from the standard method of likelihood analysis (see alternatives discussed in Sec. 3.7), but it will take substantial development for those methods to be viable.

8. Having (at least) two methods with different assumptions for any complex analysis step is highly valuable. This was highlighted in the DES year 1 cosmology analysis (DES Collaboration et al. 2017). Even having two independent pipelines that share assumptions can be useful for identifying bugs, hidden assumptions, and numerical issues. Pipeline redundancy will likely remain an important element of cosmology analysis in the 2020s, and hence it is really valuable that for most of the key issues discussed here (e.g., $N(z)$ and shear calibration) there are multiple viable approaches.

9. Null tests are valuable, but it is important to understand what really is a null test, and which "null tests" could be defeated by faulty assumptions.

10. In many of the above sections on theoretical systematics, papers that are referenced show methods for marginalizing over that systematic. Most of those papers considered individual systematics in isolation. The full problem with all of these theoretical and observational systematics is likely more complex, with degeneracies between some systematics. It will be important for the field to confront the multiple-systematics-mitigation problem sooner rather than later, in order to identify obstacles early on and develop strategies to overcome them.

The issue of multiple independent approaches raises the question of how independent the different surveys should try to be. For example, if they all rely on the representativeness of a given spectroscopic training sample for photo-z, systematic uncertainties could become correlated across the surveys. Cross-survey comparison, when carried out properly, can be a powerful tool for identifying inconsistencies that may be due to systematic errors. But it is important to consider the ingredients of the analysis (e.g., commonality in algorithms for shear calibration or photo-z calibration, same vs. different implementations of common algorithms) before deciding what parts truly are independent. In that sense, comparison against CMB lensing is "safer" as a cross-check, because it is difficult to correlate systematics between galaxy and CMB lensing. It is clear, however, that a broad set of internal cross-checks (Section 4) and external ones will be necessary for the surveys of the 2020s to produce credible weak lensing cosmology results. This work should begin before the 2020s: existing surveys – KiDS, HSC, and DES – will play a crucial role in this path towards believable precision cosmology with the surveys of the 2020s. The community must demonstrate an ability to self-consistently constrain cosmology with these datasets.

While Figure 2 (left panel) provided an initial motivation for why weak lensing is so valuable as a cosmological probe, the sections above may raise the question of why try to do it at all given the complexity of the problems involved? The community has made tremendous strides in how to address the key problems facing the field, and most outstanding issues now have multiple paths to a resolution. To distinguish between general dark energy and modified gravity models as the cause of the observed accelerated expansion rate of the Universe, we generally require a probe of the distance-redshift relation (e.g., baryon acoustic oscillations, supernovae, time-delay strong lenses) and structure growth (weak lensing, galaxy clustering, redshift-space distortions, galaxy cluster counts). While all come with challenges, weak lensing is currently the most promising of the "structure growth" probes. Use of galaxy clustering or redshift-space distortions alone requires highly precise determination of the galaxy bias or marginalization over its value (which weakens constraints). In contrast, weak lensing allows direct determination of the galaxy bias from the shear-shear, galaxy-shear, galaxy-galaxy correlations. Competitive galaxy cluster measurements of cosmology require weak lensing measurements with special care for systematics and theoretical uncertainties arising in crowded cluster regions. All probes of structure growth besides shear-shear correlations suffer worse from baryonic effects, since weak lensing signals are dominated by collisionless matter in the translinear regime. In short, these factors plus the tremendous development in the field of weak lensing in the past decade lead to the conclusion that weak lensing provides the cosmology community's best hope for competitive and believable constraints on cosmic structure growth, and hence on dark energy.

ACKNOWLEDGMENTS

LITERATURE CITED

Abazajian K, Dodelson S. 2003. *Physical Review Letters* 91:041301

Abazajian KN, Adshead P, Ahmed Z, Allen SW, Alonso D, et al. 2016. *preprint (arXiv:1610.02743)*

Abazajian KN, Calabrese E, Cooray A, De Bernardis F, Dodelson S, et al. 2011. *Astroparticle Physics* 35:177–184

Adelman-McCarthy JK, Agüeros MA, Allam SS, Anderson KSJ, Anderson SF, et al. 2006. *ApJS* 162:38–48

Aihara H, Allende Prieto C, An D, Anderson SF, Aubourg É, et al. 2011. *ApJS* 193:29

Aihara H, Arimoto N, Armstrong R, Arnouts S, Bahcall NA, et al. 2017. The Hyper Suprime-Cam SSP Survey: Overview and Survey Design

Albrecht A, Bernstein G, Cahn R, Freedman WL, Hewitt J, et al. 2006. *preprint (arXiv:astro-ph/0609591)*

Alsing J, Heavens A, Jaffe AH, Kiessling A, Wandelt B, Hoffmann T. 2016. *MNRAS* 455:4452–4466

Amara A, Réfrégier A. 2007. *MNRAS* 381:1018–1026

Amon A, Heymans C, Klaes D, Erben T, Blake C, et al. 2017. *preprints (arXiv:1707.04105)*

Antilogus P, Astier P, Doherty P, Guyonnet A, Regnault N. 2014. *Journal of Instrumentation* 9:C03048

Asgari M, Schneider P, Simon P. 2012. *A&A* 542:A122

Awan H, Gawiser E, Kurczynski P, Jones RL, Zhan H, et al. 2016. *ApJ* 829:50

Bacon DJ, Refregier AR, Ellis RS. 2000. *MNRAS* 318:625–640

Baldauf T, Smith RE, Seljak U, Mandelbaum R. 2010. *Phys. Rev. D* 81:063531

Barreira A, Llinares C, Bose S, Li B. 2016. *J. Cosmology Astropart. Phys.* 5:001

Baumer M, Davis CP, Roodman A. 2017. *PASP* 129:084502

Baxter E, Clampitt J, Giannantonio T, Dodelson S, Jain B, et al. 2016. *MNRAS* 461:4099–4114

Beck R, Lin CA, Ishida EEO, Gieseke F, de Souza RS, et al. 2017. *preprint (arXiv:1701.08748)*

Becker MR. 2013. *MNRAS* 435:115–132

Becker MR, Troxel MA, MacCrann N, Krause E, Eifler TF, et al. 2016. *Phys. Rev. D* 94:022002

Benjamin J, van Waerbeke L, Ménard B, Kilbinger M. 2010. *MNRAS* 408:1168–1180

Bergé J, Price S, Amara A, Rhodes J. 2012. *MNRAS* 419:2356–2368

Bernardeau F. 1998. *A&A* 338:375–382

Bernardeau F, Bonvin C, Vernizzi F. 2010. *Phys. Rev. D* 81:083002

Bernstein G, Huterer D. 2010. *MNRAS* 401:1399–1408

Bernstein GM. 2009. *ApJ* 695:652–665

Bernstein GM. 2010. *MNRAS* 406:2793–2804

Bernstein GM, Abbott TMC, Desai S, Gruen D, Gruendl RA, et al. 2017a. *preprint (arXiv:1706.09928)*

Bernstein GM, Armstrong R. 2014. *MNRAS* 438:1880–1893

Bernstein GM, Armstrong R, Krawiec C, March MC. 2016. *MNRAS* 459:4467–4484

Bernstein GM, Armstrong R, Plazas AA, Walker AR, Abbott TMC, et al. 2017b. *PASP* 129:074503

Bernstein GM, Jarvis M. 2002. *AJ* 123:583–618

Bertin E. 2011. *Automated Morphometry with SExtractor and PSFEx*. In *Astronomical Data Anal-

ysis Software and Systems XX, eds. IN Evans, A Accomazzi, DJ Mink, AH Rots, vol. 442 of *Astronomical Society of the Pacific Conference Series*

Blazek J, MacCrann N, Troxel MA, Fang X. 2017. *ArXiv e-prints*

Blazek J, Vlah Z, Seljak U. 2015. *J. Cosmology Astropart. Phys.* 8:015

Blot L, Corasaniti PS, Amendola L, Kitching TD. 2016. *MNRAS* 458:4462–4470

Bosch J, Armstrong R, Bickerton S, Furusawa H, Ikeda H, et al. 2017. *preprint (arXiv:1705.06766)*

Bridle S, Balan ST, Bethge M, Gentile M, Harmeling S, et al. 2010. *MNRAS* 405:2044–2061

Bridle S, Shawe-Taylor J, Amara A, Applegate D, Balan ST, et al. 2009. *Annals of Applied Statistics* 3:6–37

Burke D, Rykoff ES, Allam S, Annis J, Bechtol K, et al. 2017. *preprint (arXiv:1706.01542)*

Catelan P, Kamionkowski M, Blandford RD. 2001. *MNRAS* 320:L7–L13

Chang C, Jarvis M, Jain B, Kahn SM, Kirkby D, et al. 2013. *MNRAS* 434:2121–2135

Chang C, Marshall PJ, Jernigan JG, Peterson JR, Kahn SM, et al. 2012. *MNRAS* 427:2572–2587

Chang C, Pujol A, Mawdsley B, Bacon D, Elvin-Poole J, et al. 2017. *ArXiv e-prints*

Chisari NE, Dunkley J, Miller L, Allison R. 2015. *MNRAS* 453:682–689

Chisari NE, Koukoufilippas N, Jindal A, Peirani S, Beckmann RS, et al. 2017. *MNRAS* 472:1163–1181

Choi A, Heymans C, Blake C, Hildebrandt H, Duncan CAJ, et al. 2016. *MNRAS* 463:3737–3754

Coupon J, Arnouts S, van Waerbeke L, Moutard T, Ilbert O, et al. 2015. *MNRAS* 449:1352–1379

Croft RAC, Dailey M. 2011. *preprint (arXiv:1112.3108)*

Croft RAC, Metzler CA. 2000. *ApJ* 545:561–571

Cunha CE, Lima M, Oyaizu H, Frieman J, Lin H. 2009. *MNRAS* 396:2379–2398

Cypriano ES, Amara A, Voigt LM, Bridle SL, Abdalla FB, et al. 2010. *MNRAS* 405:494–502

Dark Energy Survey Collaboration, Abbott T, Abdalla FB, Aleksić J, Allam S, et al. 2016. *MNRAS* 460:1270–1299

Das S, Errard J, Spergel D. 2013. *preprint (arXiv:1311.2338)*

Dawson WA, Schneider MD, Tyson JA, Jee MJ. 2016. *ApJ* 816:11

de Jong JTA, Verdoes Kleijn GA, Kuijken KH, Valentijn EA. 2013. *Experimental Astronomy* 35:25–44

Decadal Survey Committee. 2010. *New Worlds, New Horizons in Astronomy and Astrophysics.* The National Academies Press

DES Collaboration, Abbott TMC, Abdalla FB, Alarcon A, Aleksić J, et al. 2017. *preprint (arXiv:1708.01530)*

Dodelson S. 2017. *Gravitational Lensing.* Cambridge University Press

Dodelson S, Schneider MD. 2013. *Phys. Rev. D* 88:063537

Dodelson S, Shapiro C, White M. 2006. *Phys. Rev. D* 73:023009

Eifler T, Krause E, Dodelson S, Zentner AR, Hearin AP, Gnedin NY. 2015. *MNRAS* 454:2451–2471

Eifler T, Schneider P, Hartlap J. 2009. *A&A* 502:721–731

Er X, Hoekstra H, Schrabback T, Cardone VF, Scaramella R, et al. 2017. *preprint (arXiv:1708.06085)*

Fenech Conti I, Herbonnet R, Hoekstra H, Merten J, Miller L, Viola M. 2017. *MNRAS* 467:1627–1651

Feroz F, Hobson MP, Bridges M. 2009. *MNRAS* 398:1601–1614

Foreman-Mackey D, Hogg DW, Lang D, Goodman J. 2013. *PASP* 125:306

Friedrich O, Eifler T. 2017. *preprint (arXiv:1703.07786)*

Fruchter AS. 2011. *PASP* 123:497

Fruchter AS, Hook RN. 2002. *PASP* 114:144–152

Gentile M, Courbin F, Meylan G. 2013. *A&A* 549:A1

Giblin Jr JT, Mertens JB, Starkman GD, Zentner AR. 2017. *preprint (arXiv:1707.06640)*

Górski KM, Banday AJ, Hivon E, Wandelt BD. 2002. *HEALPix — a Framework for High Resolution, Fast Analysis on the Sphere.* In *Astronomical Data Analysis Software and Systems XI,*

eds. DA Bohlender, D Durand, TH Handley, vol. 281 of *Astronomical Society of the Pacific Conference Series*

Gruen D, Brimioulle F. 2017. *MNRAS* 468:769–782

Gruen D, Seitz S, Brimioulle F, Kosyra R, Koppenhoefer J, et al. 2014. *MNRAS* 442:1507–1544

Gualdi D, Manera M, Joachimi B, Lahav O. 2017. *preprint (arXiv:1709.03600)*

Gurvich A, Mandelbaum R. 2016. *MNRAS* 457:3522–3534

Guyonnet A, Astier P, Antilogus P, Regnault N, Doherty P. 2015. *A&A* 575:A41

Hall A, Taylor A. 2014. *MNRAS* 443:L119–L123

Harnois-Déraps J, Tröster T, Hojjati A, van Waerbeke L, Asgari M, et al. 2016. *MNRAS* 460:434–457

Hartlap J, Hilbert S, Schneider P, Hildebrandt H. 2011. *A&A* 528:A51

Hartlap J, Simon P, Schneider P. 2007. *A&A* 464:399–404

Hearin AP, Zentner AR, Ma Z, Huterer D. 2010. *ApJ* 720:1351–1369

Heavens A, Refregier A, Heymans C. 2000. *MNRAS* 319:649–656

Heitmann K, Lawrence E, Kwan J, Habib S, Higdon D. 2014. *ApJ* 780:111

Heymans C, Heavens A. 2003. *MNRAS* 339:711–720

Heymans C, Van Waerbeke L, Bacon D, Berge J, Bernstein G, et al. 2006a. *MNRAS* 368:1323–1339

Heymans C, Van Waerbeke L, Miller L, Erben T, Hildebrandt H, et al. 2012. *MNRAS* 427:146–166

Heymans C, White M, Heavens A, Vale C, van Waerbeke L. 2006b. *MNRAS* 371:750–760

Hikage C, Takada M, Hamana T, Spergel D. 2011. *MNRAS* 412:65–74

Hilbert S, Hartlap J, White SDM, Schneider P. 2009. *A&A* 499:31–43

Hilbert S, Xu D, Schneider P, Springel V, Vogelsberger M, Hernquist L. 2017. *MNRAS* 468:790–823

Hildebrandt H, Arnouts S, Capak P, Moustakas LA, Wolf C, et al. 2010. *A&A* 523:A31

Hildebrandt H, Erben T, Kuijken K, van Waerbeke L, Heymans C, et al. 2012. *MNRAS* 421:2355–2367

Hildebrandt H, Viola M, Heymans C, Joudaki S, Kuijken K, et al. 2017. *MNRAS* 465:1454–1498

Hirata CM, Mandelbaum R, Seljak U, Guzik J, Padmanabhan N, et al. 2004. *MNRAS* 353:529–549

Hirata CM, Seljak U. 2004. *Phys. Rev. D* 70:063526–+

Hoekstra H. 2004. *MNRAS* 347:1337–1344

Hoekstra H, Herbonnet R, Muzzin A, Babul A, Mahdavi A, et al. 2015. *MNRAS* 449:685–714

Hoekstra H, Viola M, Herbonnet R. 2017. *MNRAS* 468:3295–3311

Hoyle B, Gruen D, Bernstein GM, Rau MM, De Vicente J, et al. 2017. *preprint (arXiv:1708.01532)*

Hu W. 2002. *Phys. Rev. D* 65:023003

Huang S, Leauthaud A, Murata R, Bosch J, Price P, et al. 2017. *preprint (arXiv:1705.01599)*

Hudson MJ, Gillis BR, Coupon J, Hildebrandt H, Erben T, et al. 2015. *MNRAS* 447:298–314

Huff E, Mandelbaum R. 2017. *preprint (arXiv:1702.02600)*

Huff EM, Hirata CM, Mandelbaum R, Schlegel D, Seljak U, Lupton RH. 2014. *MNRAS* 440:1296–1321

Huterer D. 2002. *Phys. Rev. D* 65:63001–+

Huterer D, Takada M. 2005. *Astroparticle Physics* 23:369–376

Ilbert O, Arnouts S, McCracken HJ, Bolzonella M, Bertin E, et al. 2006. *A&A* 457:841–856

Ilbert O, Capak P, Salvato M, Aussel H, McCracken HJ, et al. 2009. *ApJ* 690:1236–1249

Jain B, Jarvis M, Bernstein G. 2006. *J. Cosmology Astropart. Phys.* 2:001

Jain B, Spergel D, Bean R, Connolly A, Dell'antonio I, et al. 2015. *preprint (arXiv:1501.07897)*

Jarvis M, Sheldon E, Zuntz J, Kacprzak T, Bridle SL, et al. 2016. *MNRAS* 460:2245–2281

Jasche J, Wandelt BD. 2013. *ApJ* 779:15

Jee MJ, Blakeslee JP, Sirianni M, Martel AR, White RL, Ford HC. 2007. *PASP* 119:1403–1419

Jee MJ, Tyson JA, Hilbert S, Schneider MD, Schmidt S, Wittman D. 2016. *ApJ* 824:77

Jee MJ, Tyson JA, Schneider MD, Wittman D, Schmidt S, Hilbert S. 2013. *ApJ* 765:74

Joachimi B, Bridle SL. 2010. *A&A* 523:A1

Joachimi B, Cacciato M, Kitching TD, Leonard A, Mandelbaum R, et al. 2015. *Space Sci. Rev.*

193:1–65

Joachimi B, Schneider P. 2009. *A&A* 507:105–129

Johnson A, Blake C, Amon A, Erben T, Glazebrook K, et al. 2017. *MNRAS* 465:4118–4132

Joseph R, Courbin F, Starck JL. 2016. *A&A* 589:A2

Kacprzak T, Zuntz J, Rowe B, Bridle S, Refregier A, et al. 2012. *MNRAS* 427:2711–2722

Kaiser N, Squires G, Broadhurst T. 1995. *ApJ* 449:460

Kannawadi A, Shapiro CA, Mandelbaum R, Hirata CM, Kruk JW, Rhodes JD. 2016. *PASP* 128:095001

Khandai N, Di Matteo T, Croft R, Wilkins S, Feng Y, et al. 2015. *MNRAS* 450:1349–1374

Kiessling A, Cacciato M, Joachimi B, Kirk D, Kitching TD, et al. 2015. *Space Sci. Rev.* 193:67–136

Kilbinger M. 2015. *Reports on Progress in Physics* 78:086901

Kilbinger M, Heymans C, Asgari M, Joudaki S, Schneider P, et al. 2017. *preprint (arXiv:1702.05301)*

Kilbinger M, Schneider P, Eifler T. 2006. *A&A* 457:15–19

King L, Schneider P. 2002. *A&A* 396:411–418

Kirk D, Brown ML, Hoekstra H, Joachimi B, Kitching TD, et al. 2015. *Space Sci. Rev.* 193:139–211

Kitching T, Balan S, Bernstein G, Bethge M, Bridle S, et al. 2010. *AOAS* 5:2231–2263

Kitching TD, Alsing J, Heavens AF, Jimenez R, McEwen JD, Verde L. 2017. *MNRAS* 469:2737–2749

Kitching TD, Balan ST, Bridle S, Cantale N, Courbin F, et al. 2012. *MNRAS* 423:3163–3208

Kitching TD, Heavens AF, Alsing J, Erben T, Heymans C, et al. 2014. *MNRAS* 442:1326–1349

Kitching TD, Heavens AF, Miller L. 2011. *MNRAS* 413:2923–2934

Kitching TD, Rowe B, Gill M, Heymans C, Massey R, et al. 2013. *ApJS* 205:12

Krause E, Eifler T, Blazek J. 2016. *MNRAS* 456:207–222

Krause E, Eifler TF, Zuntz J, Friedrich O, Troxel MA, et al. 2017. *preprint (arXiv:1706.09359)*

Krause E, Hirata CM. 2010. *A&A* 523:A28

Lage C, Bradshaw A, Tyson JA. 2017. *Journal of Instrumentation* 12:C03091

Landy SD, Szalay AS. 1993. *ApJ* 412:64–71

Lauer TR. 1999. *PASP* 111:227–237

Laureijs R, Amiaux J, Arduini S, Auguères J, Brinchmann J, et al. 2011. *preprint (astro-ph:1110.3193)*

Leauthaud A, Massey R, Kneib J, Rhodes J, Johnston DE, et al. 2007. *ApJS* 172:219–238

Lee J, Pen U. 2000. *ApJ* 532:L5–L8

Lee J, Pen U. 2001. *ApJ* 555:106–124

Lemos P, Challinor A, Efstathiou G. 2017. *J. Cosmology Astropart. Phys.* 5:014

Lewis A, Bridle S. 2002. *Phys. Rev. D* 66:103511–+

Li TS, DePoy DL, Marshall JL, Tucker D, Kessler R, et al. 2016. *AJ* 151:157

Li Y, Hu W, Takada M. 2014. *Phys. Rev. D* 89:083519

Lima M, Cunha CE, Oyaizu H, Frieman J, Lin H, Sheldon ES. 2008. *MNRAS* 390:118–130

Lin CA, Kilbinger M. 2015. *A&A* 583:A70

LSST Science Collaboration, Abell PA, Allison J, Anderson SF, Andrew JR, et al. 2009. *preprints (astro-ph:0912.0201)*

LSST Science Collaboration, Marshall P, Anguita T, Bianco FB, Bellm EC, et al. 2017. *ArXiv e-prints*

Lu T, Zhang J, Dong F, Li Y, Liu D, et al. 2017. *AJ* 153:197

Ma Z, Bernstein G. 2008. *ApJ* 682:39–48

Mandelbaum R, Hirata CM, Seljak U, Guzik J, Padmanabhan N, et al. 2005. *MNRAS* 361:1287–1322

Mandelbaum R, Lanusse F, Leauthaud A, Armstrong R, Simet M, et al. 2017a. *preprint (arXiv:1710.00885)*

Mandelbaum R, Miyatake H, Hamana T, Oguri M, Simet M, et al. 2017b. *preprint (arXiv:1705.06745)*

Mandelbaum R, Rowe B, Armstrong R, Bard D, Bertin E, et al. 2015. *MNRAS* 450:2963–3007

Mandelbaum R, Rowe B, Bosch J, Chang C, Courbin F, et al. 2014. *ApJS* 212:5

Mandelbaum R, Slosar A, Baldauf T, Seljak U, Hirata CM, et al. 2013. *MNRAS* 432:1544–1575

Mandelbaum R, Wang W, Zu Y, White S, Henriques B, More S. 2016. *MNRAS* 457:3200–3218

Marian L, Smith RE, Angulo RE. 2015. *MNRAS* 451:1418–1444

Massey R, Heymans C, Bergé J, Bernstein G, Bridle S, et al. 2007a. *MNRAS* 376:13–38

Massey R, Hoekstra H, Kitching T, Rhodes J, Cropper M, et al. 2013. *MNRAS* 429:661–678

Massey R, Rowe B, Refregier A, Bacon DJ, Bergé J. 2007b. *MNRAS* 380:229–245

Massey R, Stoughton C, Leauthaud A, Rhodes J, Koekemoer A, et al. 2010. *MNRAS* 401:371–384

Masters D, Capak P, Stern D, Ilbert O, Salvato M, et al. 2015. *ApJ* 813:53

Masters DC, Stern DK, Cohen JG, Capak PL, Rhodes JD, et al. 2017. *ApJ* 841:111

McEwen JE, Weinberg DH. 2016. *preprint (arXiv:1601.02693)*

McQuinn M, White M. 2013. *MNRAS* 433:2857–2883

Mead AJ, Peacock JA, Heymans C, Joudaki S, Heavens AF. 2015. *MNRAS* 454:1958–1975

Medezinski E, Oguri M, Nishizawa AJ, Speagle JS, Miyatake H, et al. 2017. *preprint (arXiv:1706.00427)*

Melchior P, Böhnert A, Lombardi M, Bartelmann M. 2010. *A&A* 510:A75

Melchior P, Gruen D, McClintock T, Varga TN, Sheldon E, et al. 2017. *MNRAS* 469:4899–4920

Melchior P, Viola M. 2012. *MNRAS* 424:2757–2769

Ménard B, Scranton R, Schmidt S, Morrison C, Jeong D, et al. 2013. *preprint (astro-ph:1303.4722)*

Meyers JE, Burchat PR. 2015a. *Journal of Instrumentation* 10:C06004

Meyers JE, Burchat PR. 2015b. *ApJ* 807:182

Miller L, Heymans C, Kitching TD, van Waerbeke L, Erben T, et al. 2013. *MNRAS* 429:2858–2880

Mohammed I, Seljak U. 2014. *MNRAS* 445:3382–3400

Mohammed I, Seljak U, Vlah Z. 2017. *MNRAS* 466:780–797

More S, Miyatake H, Mandelbaum R, Takada M, Spergel DN, et al. 2015. *ApJ* 806:2

Morrison CB, Hildebrandt H. 2015. *MNRAS* 454:3121–3133

Morrison CB, Hildebrandt H, Schmidt SJ, Baldry IK, Bilicki M, et al. 2017. *MNRAS* 467:3576–3589

Morrison CB, Schneider MD. 2013. *J. Cosmology Astropart. Phys.* 11:009

Newman JA. 2008. *ApJ* 684:88–101

Newman JA, Abate A, Abdalla FB, Allam S, Allen SW, et al. 2015. *Astroparticle Physics* 63:81–100

Oguri M, Miyazaki S, Hikage C, Mandelbaum R, Utsumi Y, et al. 2017. *preprint (arXiv:1705.06792)*

Padmanabhan N, White M, Zhou HH, O'Connell R. 2016. *MNRAS* 460:1567–1576

Paulin-Henriksson S, Amara A, Voigt L, Refregier A, Bridle SL. 2008. *A&A* 484:67–77

Petri A, Haiman Z, May M. 2017. *Phys. Rev. D* 95:123503

Planck Collaboration, Ade PAR, Aghanim N, Armitage-Caplan C, Arnaud M, et al. 2014. *A&A* 571:A17

Plazas AA, Bernstein G. 2012. *PASP* 124:1113

Plazas AA, Bernstein GM, Sheldon ES. 2014. *PASP* 126:750

Plazas AA, Shapiro C, Kannawadi A, Mandelbaum R, Rhodes J, Smith R. 2016. *PASP* 128:104001

Plazas AA, Shapiro C, Smith R, Rhodes J, Huff E. 2017. *Journal of Instrumentation* 12:C04009

Rasmussen A, Antilogus P, Astier P, Claver C, Doherty P, et al. 2014. *A framework for modeling the detailed optical response of thick, multiple segment, large format sensors for precision astronomy applications.* In *Modeling, Systems Engineering, and Project Management for Astronomy VI*, vol. 9150 of *Proc. SPIE*

Refregier A, Kacprzak T, Amara A, Bridle S, Rowe B. 2012. *MNRAS* 425:1951–1957

Rhodes J, Leauthaud A, Stoughton C, Massey R, Dawson K, et al. 2010. *PASP* 122:439

Rhodes J, Refregier A, Groth EJ. 2001. *ApJ* 552:L85–L88

Rhodes JD, Massey RJ, Albert J, Collins N, Ellis RS, et al. 2007. *ApJS* 172:203–218

Roodman A, Reil K, Davis C. 2014. *Wavefront sensing and the active optics system of the dark energy camera.* In *Ground-based and Airborne Telescopes V*, vol. 9145 of *Proc. SPIE*

Rowe B. 2010. *MNRAS* 404:350–366

Rowe B, Hirata C, Rhodes J. 2011. *ApJ* 741:46

Rowe BTP, Jarvis M, Mandelbaum R, Bernstein GM, Bosch J, et al. 2015. *Astronomy and Computing* 10:121–150

Samuroff S, Bridle SL, Zuntz J, Troxel MA, Gruen D, et al. 2017. *preprint (arXiv:1708.01534)*

Sánchez C, Carrasco Kind M, Lin H, Miquel R, Abdalla FB, et al. 2014. *MNRAS* 445:1482–1506

Sato M, Hamana T, Takahashi R, Takada M, Yoshida N, et al. 2009. *ApJ* 701:945–954

Sato M, Takada M, Hamana T, Matsubara T. 2011. *ApJ* 734:76

Schaan E, Krause E, Eifler T, Doré O, Miyatake H, et al. 2017. *Phys. Rev. D* 95:123512

Schaye J, Crain RA, Bower RG, Furlong M, Schaller M, et al. 2015. *MNRAS* 446:521–554

Schmidt SJ, Ménard B, Scranton R, Morrison C, McBride CK. 2013. *MNRAS* 431:3307–3318

Schneider MD, Cole S, Frenk CS, Szapudi I. 2011. *ApJ* 737:11

Schneider MD, Frenk CS, Cole S. 2012. *J. Cosmology Astropart. Phys.* 5:030

Schneider MD, Hogg DW, Marshall PJ, Dawson WA, Meyers J, et al. 2015. *ApJ* 807:87

Schneider P, van Waerbeke L, Kilbinger M, Mellier Y. 2002. *A&A* 396:1–19

Schneider P, van Waerbeke L, Mellier Y. 2002. *A&A* 389:729–741

Schrabback T, Hartlap J, Joachimi B, Kilbinger M, Simon P, et al. 2010. *A&A* 516:A63+

Scranton R, Krughoff KS, Connolly AJ. 2007. *Chapter 10: Web-based Tools - STOMP Footprint Service*. In *Astronomical Society of the Pacific Conference Series*, eds. MJ Graham, MJ Fitzpatrick, TA McGlynn, vol. 382 of *Astronomical Society of the Pacific Conference Series*

Sellentin E, Heavens AF. 2017. *MNRAS* 464:4658–4665

Semboloni E, Hoekstra H, Schaye J, van Daalen MP, McCarthy IG. 2011. *MNRAS* 417:2020–2035

Seshadri S, Shapiro C, Goodsall T, Fucik J, Hirata C, et al. 2013. *PASP* 125:1065

Sheldon E. 2015. NGMIX: Gaussian mixture models for 2D images. Astrophysics Source Code Library

Sheldon ES, Huff EM. 2017. *ApJ* 841:24

Sheldon ES, Johnston DE, Frieman JA, Scranton R, McKay TA, et al. 2004. *AJ* 127:2544–2564

Shirasaki M, Takada M, Miyatake H, Takahashi R, Hamana T, et al. 2017. *MNRAS* 470:3476–3496

Simet M, Mandelbaum R. 2015. *MNRAS* 449:1259–1269

Simon P, Taylor AN, Hartlap J. 2009. *MNRAS* 399:48–68

Singh S, Mandelbaum R. 2016. *MNRAS* 457:2301–2317

Singh S, Mandelbaum R, Brownstein JR. 2017. *MNRAS* 464:2120–2138

Singh S, Mandelbaum R, Seljak U, Slosar A, Vazquez Gonzalez J. 2017. *MNRAS* 471:3827–3844

Sirianni M, Clampin M, Hartig GF, Rafal MD, Ford HC, et al. 1998. *Long-wavelength scattered-light halos in ASC CCDs*. In *Optical Astronomical Instrumentation*, ed. S D'Odorico, vol. 3355 of *Proc. SPIE*

Soo JYH, Moraes B, Joachimi B, Hartley W, Lahav O, et al. 2017. *preprint (arXiv:1707.03169)*

Spergel D, Gehrels N, Baltay C, Bennett D, Breckinridge J, et al. 2015. *preprint (arXiv:1503.03757)*

Stetson PB. 1987. *PASP* 99:191–222

Suchyta E, Huff EM, Aleksić J, Melchior P, Jouvel S, et al. 2016. *MNRAS* 457:786–808

Sun L, Fan ZH, Tao C, Kneib JP, Jouvel S, Tilquin A. 2009. *ApJ* 699:958–967

Swanson M, Tegmark M, Hamilton A, Hill C. 2012. Mangle: Angular Mask Software. Astrophysics Source Code Library

Takahashi R, Sato M, Nishimichi T, Taruya A, Oguri M. 2012. *ApJ* 761:152

Tanaka M, Coupon J, Hsieh BC, Mineo S, Nishizawa AJ, et al. 2017. *preprint (arXiv:1704.05988)*

Taylor A, Joachimi B, Kitching T. 2013. *MNRAS* 432:1928–1946

Tenneti A, Mandelbaum R, Di Matteo T. 2016. *MNRAS* 462:2668–2680

Troxel MA, Ishak M. 2014. *Phys. Rev. D* 89:063528

Troxel MA, Ishak M. 2015. *Phys. Rep.* 558:1–59

Troxel MA, MacCrann N, Zuntz J, Eifler TF, Krause E, et al. 2017. *preprint (arXiv:1708.01538)*

Tyson JA, Roat C, Bosch J, Wittman D. 2008. *LSST and the Dark Sector: Image Processing*

Challenges. In *Astronomical Data Analysis Software and Systems XVII*, ed. R. W. Argyle, P. S. Bunclark, & J. R. Lewis, vol. 394 of *Astronomical Society of the Pacific Conference Series*

Tyson JA, Sasian J, Gilmore K, Bradshaw A, Claver C, et al. 2014. *LSST optical beam simulator*. In *High Energy, Optical, and Infrared Detectors for Astronomy VI*, vol. 9154 of *Proc. SPIE*

Vallinotto A. 2012. *ApJ* 759:32

van den Bosch FC, More S, Cacciato M, Mo H, Yang X. 2013. *MNRAS* 430:725–746

van Uitert E, Cacciato M, Hoekstra H, Herbonnet R. 2015. *A&A* 579:A26

van Uitert E, Joachimi B, Joudaki S, Heymans C, Köhlinger F, et al. 2017. *preprint (arXiv:1706.05004)*

Van Waerbeke L, Mellier Y, Erben T, Cuillandre JC, Bernardeau F, et al. 2000. *A&A* 358:30–44

Velliscig M, Cacciato M, Schaye J, Hoekstra H, Bower RG, et al. 2015. *MNRAS* 454:3328–3340

Vogelsberger M, Genel S, Springel V, Torrey P, Sijacki D, et al. 2014. *Nature* 509:177–182

Voigt LM, Bridle SL. 2010. *MNRAS* 404:458–467

Voigt LM, Bridle SL, Amara A, Cropper M, Kitching TD, et al. 2012. *MNRAS* 421:1385–1398

Wittman DM, Tyson JA, Kirkman D, Dell'Antonio I, Bernstein G. 2000. *Nature* 405:143–148

Xin B, Roodman A, Angeli G, Claver C, Thomas S. 2016. *Comparison of LSST and DECam wavefront recovery algorithms*. In *Ground-based and Airborne Telescopes VI*, vol. 9906 of *Proc. SPIE*

Yao J, Ishak M, Lin W, Troxel MA. 2017. *preprint (arXiv:1707.01072)*

Yoo J, Tinker JL, Weinberg DH, Zheng Z, Katz N, Davé R. 2006. *ApJ* 652:26–42

Zentner AR, Semboloni E, Dodelson S, Eifler T, Krause E, Hearin AP. 2013. *Phys. Rev. D* 87:043509

Zhang J, Komatsu E. 2011. *MNRAS* 414:1047–1058

Zhang Y, McKay TA, Bertin E, Jeltema T, Miller CJ, et al. 2015. *PASP* 127:1183

Zuntz J, Sheldon E, Samuroff S, Troxel MA, Jarvis M, et al. 2017. *preprint (arXiv:1708.01533)*